Front. Med. 2025, 19(6): 1194−1213
https://doi.org/10.1007/s11684-025-1175-x

RESEARCH ARTICLE

A specific tsRNA in serum from patients with nasopharyngeal carcinoma: 5′tiRNA-32-ValAAC-2 mediates malignance of nasopharyngeal carcinoma cells

Qi Tang[1,2], Yao Wu[1], Lin Chen[1], Qunying Jia[2], Yingchun He[1], Faqing Tang (✉)[1,2]

[1]The First Hospital of Hunan University of Chinese Medicine, Changsha 410208, China; [2]Department of Clinical Laboratory and Hunan Key Laboratory of Oncotarget gene, Hunan Cancer Hospital, and The Affiliated Cancer Hospital of Xiangya School of Medicine, Central South University, Changsha 410013, China

Abstract **Early diagnosis is vitally important for effective treatment of nasopharyngeal carcinoma (NPC). Nevertheless, the exact pathogenic mechanisms of NPC remain unclear, and early diagnosis of NPC is still limited. Herein, we showed that a specific tsRNA for NPC, 5′tiRNA-32-ValAAC-2, is a novel pathogenic factor and has potential diagnostic value for NPC screening. In this study, small RNA microarray profiling and array hybridization were used to detect expression spectrums of tsRNAs in the sera of newly diagnosed NPC patients. The upregulated tsRNAs were validated using RT-qPCR, and their clinical significance in NPC diagnosis was analyzed. Furthermore, the most highly expressed tsRNA, was further investigated. 5′tiRNA-32-ValAAC-2 could serve as a potential diagnostic biomarker for NPC. Subsequently, the effect of 5′tiRNA-32-ValAAC-2 on the growth and invasion of NPC cells was investigated. The results indicated that overexpression of 5′tiRNA-32-ValAAC-2 promoted NPC cells proliferation, migration, and invasion. In contrast, the inhibition of 5′tiRNA-32-ValAAC-2 suppressed NPC cells proliferation, migration and invasion. TargetScan and miRanda analyses revealed that *UGT2B7*, *SYNPO2*, *ZNF44*, *PDHB*, and *UFM1* might serve as downstream target-genes of 5′tiRNA-32-ValAAC-2. In conclusion, 5′tiRNA-32-ValAAC-2 could potentially be a novel pathogenic factor for NPC, and it functions as a diagnostic biomarker in the primary diagnosis of NPC.**

Keywords 5′tiRNA-32-ValAAC-2; tsRNA; nasopharyngeal carcinoma; diagnosis; biomarker

Introduction

Nasopharyngeal carcinoma (NPC) occurs mainly in south-east Asia and the south of China [1]. According to the latest China's cancer statistics, there are more than 50 000 new cases and 20 000 deaths of NPC per year. The incidence is the highest in southern China, accounting for 47% of new cases worldwide [2]. The main treatments of NPC patients include radiotherapy, chemotherapy, concurrent chemoradiotherapy, targeted therapy, and immunotherapy, and radiotherapy or concurrent chemoradiotherapy is the first choice for NPC patients [3]. However, its therapeutic efficacy is limited in advanced stages. In contrast, early diagnosis can enhance therapeutic effect. Therefore, it becomes urgent to identify appropriate diagnosis indicators and therapeutic targets for improving survival rate of NPC patients. The etiopathogenesis of NPC is intricate, encompassing diverse factors like genetic predisposition, Epstein-Barr virus (EBV) infection, environmental elements, and pathogenic agents [4]. It is worth mentioning that tRNA-derived small RNAs (tsRNAs) are one of the important pathogenic factors in NPC. Recent researches showed that tsRNAs may become the novel diagnostic biomarkers for NPC [5,6]. Therefore, understanding the targets of tsRNA in NPC is crucial for elucidating the underlying mechanism of tsRNA in NPC and may provide novel therapeutic targets for NPC. That may greatly help with early diagnosis for early-stage disease treatment or even prevent disease onset.

tsRNAs are a newly discovered class of non-coding RNAs. These tsRNAs are derived from mature tRNAs or tRNA precursors. They function through regulating protein translation, RNA transcription, or post-transcriptional regulation [7]. tsRNAs constitute a newly

Received May 28, 2025; accepted August 14, 2025
Correspondence: Faqing Tang, tangfq@hnca.org.cn

identified class of small non-coding RNAs that are generated through the cleavage of mature tRNA or tRNA precursors by enzymes, including angiogenin, Dicer, RNase Z, and RNase P [8]. Precursor tRNAs (pre-tRNAs), each having a 5′ leading sequence and a 3′ tail region, can be transcribed from tRNA genes through the action of RNA polymerase III (RNA Pol III) [9]. Typically, RNase P removes the 5′ leader sequence [10], while RNase Z eliminates the 3′ trailing sequence [11]. The nucleotide transferase then attaches the "CCA" sequence to the 3′ end [12]. Subsequently, through post-transcriptional modification, this sequence folds into the secondary cloverleaf structure of mature tRNA. Based on their length and sites of cleavage, tsRNAs are mainly divided into two types, tRNA half-molecules (tRNA halves) and tRNA-derived RNA fragments (tRFs) [13]. tRNA halves, whose length is 29–50 nt, are induced by stress or starvation and produced by specific cleavage at the mature tRNA anticodon loop [14]. Therefore, tRNA halves can be classified into two subgroups: (1) 5′-half, ranging from the 5′ end to the anticodon loop, 30–35 nt in length; (2) 3′-half, ranging from the anticodon loop to the 3′ end, 40–50 nt in length [15]. Oxidative stress, hypoxia, and viral infection are related to the main mechanisms of tsRNA halves [16]. For another type, tRFs, tRFs are generated when cleavage mainly occurs in the anticodon loop of mature tRNA to produce 5′- and 3′-fragments that are 31–40 nt long [17]. Depending on the sources, tRFs can be divided into tRF-1, tRF-2, tRF-3, tRF-5, and i-tRF [18]. tRF-1 is derived from the 3′ end of precursor tRNA cleaved by RNase Z or its cytoplasmic homolog ribonuclease Z2 [19]. tRF-2 is decomposed from the anticodon loop of tRNA, excluding the 5′ end and the 3′ end structures. Specifically, it is induced under hypoxic conditions [20]. tRF-3, starting at the trinucleotide "CCA" at the 3′ end, originates at the 3′ end and are cleaved by Dicer and angiogenin at the T-loop of mature tRNAs. Moreover, tRF-3 is approximately 18-22 nt in length [21]. At the 5′ end of mature tRNAs, tRF-5 is cleaved by Dicer at the D-loop, D stem or 5′ anticodon stem half of tRNAs [22]. i-tRF is derived from the internal region of mature tRNAs and do not reach their 5′ end and 3′ end [23]. tRFs can bind to RNA binding proteins [24] and then target mRNA expression to control mRNA stability [25]. On the other hand, tsRNA influences the translation process by either inhibiting or facilitating protein synthesis [26].

tsRNA is ubiquitously present in diverse organisms and features high conservation, a stable structure, and tissue-specific expression. Acting as epigenetic regulators, it exerts a crucial influence on biological processes by modulating transcript stability and translation [27]. For example, the fragment derived from $tRNA^{Glu}$ induced by aging can impair the biosynthesis of glutamate by targeting the cristae organization dependent on mitochondrial translation [28], and embryonic EVs containing specific tRFs may regulate preimplantation embryo development [29]. tsRNA holds potential as a biomarker for disease and a therapeutic target, emerging as a burgeoning area of research in the biomedical field. In particular, tiRNA-Val-CAC-2 can act as promising prognostic biomarkers and potential therapeutic targets for pancreatic cancer [30]. tRFdb-3013a/b might serve as novel biomarkers for diagnosis and prognosis of colon adenocarcinomas [31], hepatocellular carcinoma [32], renal cell carcinoma [33], and gastric cancer [34]. To date, the evidence regarding tsRNA in NPC remains scanty, and only a limited number of studies have been published in this area. Little is known about the underlying mechanisms of tsRNA biogenesis and regulation in NPC, as well as the role it plays in gene regulation. Whether tsRNA can serve as a novel biomarker for the early screening of NPC requires further exploration.

5′tiRNA-32-ValAAC-2 is a member of the 5′tiRNA family. Research has indicated that it participates in cell senescence [35], protein synthesis [36], autophagic activity [37], metabolism modulation [38], gene regulation [39], and epigenetics [40]. Our small RNA chip screening data in this study has verified that 5′tiRNA constitutes 17.53% of NPC. This novel discovery has drawn significant attention from researchers. To clarify the function of tsRNA in NPC development and verify its feasibility as a marker for NPC screening, therefore, small RNA microarray profiling and array hybridization were used to detect expression spectrums of tsRNAs in serum from primary NPC patient. This study found that 5′tiRNA-32-ValAAC-2 was highly expressed in the serum of NPC patients, and it was confirmed that 5′tiRNA-32-ValAAC-2 was valuable for the primary diagnosis of NPC. Moreover, the mechanism investigation revealed that overexpression of 5′tiRNA-32-ValAAC-2 enhanced the proliferation, migration, and invasion capabilities of NPC cells, whereas knock down of 5′tiRNA-32-ValAAC-2 inhibited the growth, clone formation, migration, and invasion of NPC cells. 5′tiRNA-32-ValAAC-2 might serve as a novel pathogenic factor, and its latent worth was emphasized as a promising biomarker for the diagnosis of NPC. This research process is depicted in Fig. 1.

Materials and methods

Serum samples

From March 2024 to December 2024, serum samples were collected from 120 newly-diagnosed NPC patients and 25 normal individuals who had undergone routine physical examination at Hunan Cancer Hospital. The normal individuals served as the control group, and the

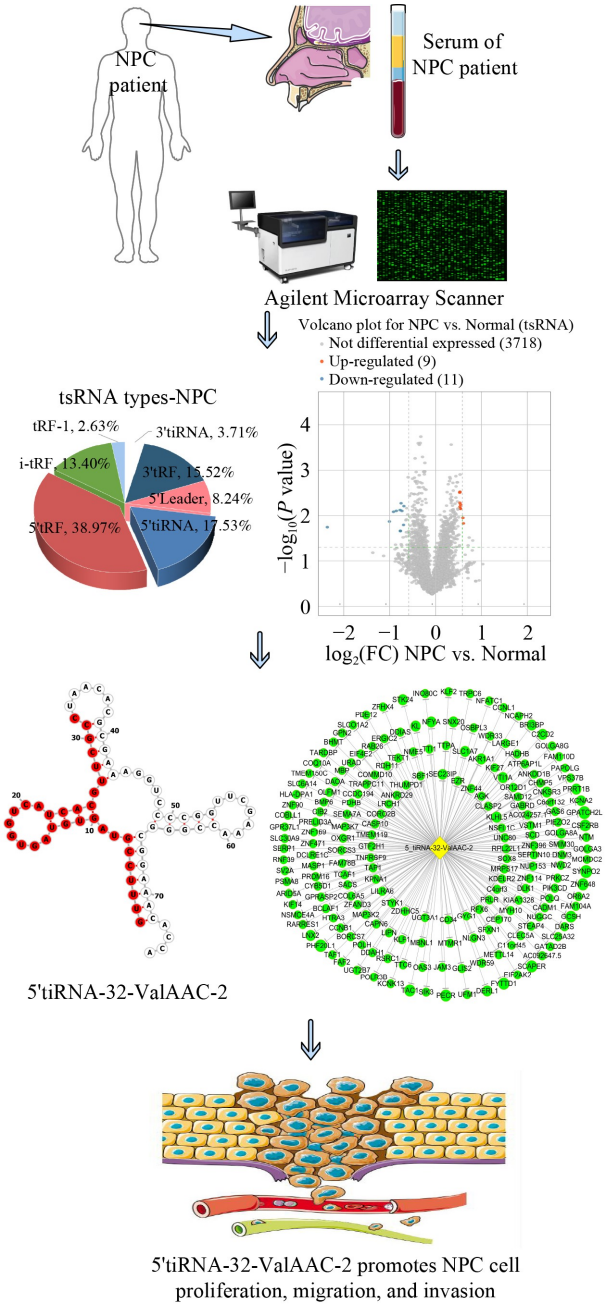

Fig. 1 The flowchart of this study.

NPC patients were the experimental group. The NPC patients were diagnosed clinically, pathologically, and radiologically. Table 1 presents the corresponding clinicopathological information along with the baseline characteristics. In this study, the pathological grade and stage of the NPC patients were determined according to the 8th-edition TNM staging method adopted by the Union for International Cancer Control (UICC) and the American Joint Committee on Cancer (AJCC). The inclusion criteria for this study are as follows. (1) Patients are diagnosed with NPC through imaging examination and pathological diagnosis. (2) The age ranges from 18 to 80 years old, with no gender limitation. (3) Patients newly diagnosed with NPC have not received any treatment. (4) Patients with detailed medical records. (5) Patients have fully understood and voluntarily signed a written informed consent form for this study. On the other hand, the exclusion criteria for this study are as follows. (1) Nasopharyngeal cancer patients not meeting the above inclusion criteria. (2) Patients currently undergoing chemotherapy, radiotherapy, targeted therapies, and other immunotherapies. (3) Patients with other serious and uncontrolled systemic diseases like cardiovascular, liver, and kidney diseases. (4) Individuals who suffer from mental illness, severe cognitive impairment or speech-expression defects and are unable to cooperate. (5) Pregnant or lactating women. (6) Patients with other malignant tumors. This study was reviewed and approved by the Ethics Committee of the Hunan Cancer Hospital and Institute (No.2024 [30], Supplementary File 1). The blood samples were collected from each participant using 5 mL vacuum blood collection tubes without anticoagulant or coagulant. After being left at room temperature for 30 min, the blood samples were first centrifuged at 3000 rpm for 10 min, and the supernatant was pipetted into a new 1.5 mL EP tube. Then samples were centrifuged at 12 000 rpm for 10 min at 4 °C, again, suck the serum into a new 1.5 mL EP tube. Serum samples were stored at −80 °C for subsequent experiments.

RNA extraction

According to the manufacturer's instructions, we isolated total RNA using TRIzol Reagent (15596026CN, Invitrogen, CA, USA). The quantity of each RNA sample was checked using the Ultramicro biodetector (BIODRPOULIFE, Thermo Scientific, MA, USA), and the integrity of RNA was assessed using agarose gel (2%, w/v) electrophoresis. For each sample, a total of 100 ng RNA was subjected to dephosphorylation to form a unified 3-OH end. The RNA with 3-OH ends was then denatured using DMSO and enzymatically labeled with Cy3. Subsequently, the Cy3-labeled small RNAs were hybridized to Arraystar Human Small RNA Arrays in Agilent Hybridization Oven (42 ℃, 12 h).

RNA labeling

In the Small RNA Microarray profiling (5190, Agilent, USA) assay, 100 ng of total RNA was first dephosphorylated with 3 units of T4 polynucleotide kinase (T4PNK) at 37 °C for 40 min. This process aimed to eliminate both (P) and (cP) chemical groups from the 3′ end of RNA, resulting in the formation of a 3-OH end. The reaction was terminated at 70 °C for 5 min and then cooled immediately to 0 °C. Subsequently, 7 μL of

Table 1 Clinical data with baseline characteristics of NPC patients

Patient ID	Gender	Age (year)	Histology	Pathological grade	Pathological stage	Ki-67	EBER
1	Male	49	Non-keratinous carcinoma, differentiated type	T1N1M0	II	80%	+
2	Female	51	Non-keratinous carcinoma, undifferentiated type	T2N3M1	IVb	60%–70%	+
3	Male	37	Non-keratinous carcinoma, undifferentiated type	T2N1M0	II	60%	+
4	Female	60	Non-keratinous carcinoma, undifferentiated type	T2N3M0	IVa	40%	+
5	Male	46	Non-keratinous carcinoma, undifferentiated type	T2N3M0	IVa	20%	+
6	Male	51	Non-keratinous carcinoma, undifferentiated type	T4N3M0	IVa	50%	+
7	Male	58	Non-keratinous carcinoma	T3N3M1	IVb	50%	+
8	Male	32	Non-keratinous carcinoma, undifferentiated type	T3N1M0	III	40%–50%	+
9	Female	50	Non-keratinous carcinoma, undifferentiated type	T2N1M0	II	50%	+
10	Male	45	Non-keratinous carcinoma, undifferentiated type	T3N3M0	IVa	40%	+
11	Male	56	Non-keratinous carcinoma, undifferentiated type	T4N1M0	IVa	30%	+
12	Male	51	Non-keratinous carcinoma, undifferentiated type	T4N3M0	IVa	60%	+
13	Female	65	Non-keratinous carcinoma, undifferentiated type	T2N2M0	III	50%	+
14	Female	65	Non-keratinous carcinoma, undifferentiated type	T2N3M0	IVa	40%	+
15	Male	68	Moderately differentiated squamous cell carcinoma	T2N0M0	II	80%	+
16	Male	61	Non-keratinous carcinoma, undifferentiated type	T3N1M0	III	80%	+
17	Female	46	Non-keratinous carcinoma, undifferentiated and differentiated mixed type	T3N2M0	III	30%	+
18	Male	41	Non-keratinous carcinoma, undifferentiated type	T2N2M0	II	70%	+
19	Male	54	Non-keratinous carcinoma, undifferentiated type	T4N2M0	IVa	80%	+
20	Male	57	Non-keratinous carcinoma, undifferentiated type	T1N3M0	IVa	40%	+

dimethyl sulfoxide (DMSO) was added and the mixture was heated to 100 °C for 3 min to unfold the RNA, followed by immediate chilling to 0 °C. RNA end labeling was performed by adding ligase buffer, bovine serum albumin (BSA), a final concentration of 50 mmol/L pCp-Cy3, and 15 units of T4 RNA ligase in a total volume of 28 μL, and then the reaction mixture was incubated at 16 °C overnight.

Array hybridization

Mix 22.5 μL 2× Hybridization buffer (G2445A, Agilent, USA) with the completed labeling reaction solution until the final volume reached 45 μL. Heat the resulting mixture at 100 °C for 5 min, then chill immediately to 0 °C. Next, 45 μL labeled sample mix was hybridized onto a microarray at 55 °C for 20 h. The slides were washed in 6× SSC containing 0.005% Triton X-102 at room temperature for 10 min, then by immersion in 0.1× SSC with 0.005% Triton X-102 for 5 min. After the washing process, the slides were scanned on an Agilent G2539A microarray scanner (5188, Agilent, USA).

tsRNA data analysis

The scanned microarray images were imported into Agilent Feature Extraction software to extract raw intensity data. The probe signals passing "P" (Present) or "M" (Marginal) QC flags in at least 5 samples were selected for further analysis. Quality normalization was performed using Agilent GeneSpring GX 12.1 software, and the normalized intensities were $\log_2$ transformed. After normalization and signal QC flag filtering, the probe signals for the same small RNA biotype were grouped and analyzed correspondingly. We averaged the normalized intensities of multiple probes for the same small RNA and combined them into an RNA level. Then, compare two groups in terms of differential small RNA expression. For each small RNA, the fold change (FC) was calculated. And the statistical significance of the difference (*P*-value) was also calculated. The default thresholds were set as FC $\geq$ 1.5 and $P < 0.05$. Based on these thresholds, differentially expressed small RNAs were annotated with genomic and biological information, and analyzed through scatter plot, volcano plot and hierarchical clustering heatmap.

Hierarchical clustering heatmaps, scatter plots and volcano plots

The samples were grouped through clustering analysis based on the similarities in small RNA expression and the

proximity of their relationships, which were shown in the dendrogram above the heatmaps. The expression levels were depicted using a color gradient and visually presented via color scales. The scatter plots depict the normalized intensities of each small RNA in the two samples being compared or group-averaged normalized intensities in the two groups being compared on the X and Y axes. It can be used to visualize, at the abundance levels (normalized intensities), the differentially expressed small RNAs (data point distances off the diagonal lines). For each small RNA comparison between the two groups (each group must have more than 2 replicates), the Volcano plot was constructed by plotting $-\log_{10}P$ as the differential significance on the Y-axis and $\log_2$(FC) as the differential magnitude on the X-axis. Thus, small RNAs with large differential significance and large magnitudes (colored in the Volcano plot) were the most likely differentially expressed small RNAs.

To determine the potential target genes of the validated tsRNAs, the database of TargetScan was filtered; then the target genes were predicted by Miranda.

RT-qPCR

From the differential sequencing results, 9 tsRNAs that were significantly upregulated and met specific primer design requirements were selected for verification. First, the expression of 9 tsRNAs was validated through RT-qPCR in the sera from 20 NPC patients and 5 normal individuals whose sera had been sequenced. Then, the potentially key tsRNAs were screened out and further validated through RT-qPCR in the sera from 100 newly-diagnosed NPC patients compared with 20 normal individuals. Total RNA was extracted from serum as previously described. Based on the manufacturer's protocols, RNA was synthesized into cDNA using miRNA 1st strand cDNA synthesis kit (Stem-loop) (AG11743, AG, China). *U6* was used as an internal control for tsRNA. The primers for *U6*, 5′tiRNA-32-ValAAC-2, tRF5-50-GlyGCC-2, i-tRF-4:24-His-GTG-1, i-tRF-2:25-His-GTG-1, 5′tiRNA-35-GlnTTG-6, tRF5-31-HisGTG-1, tRF5-23-HisGTG-1, 5′tiRNA-34-GlnTTG-6, mt-tRF5-26-Leu-TAA were designed at the website of store.sangon.com/primerDesign and are shown in Table S1. RT-qPCR was performed on the LIGHTCYCLE 96 (Roche, Germany) using 2× Universal Blue SYBR Green qPCR Master Mix (G3326-15, Servicebio, China). PCR reaction was performed using a 20 μL volume, which consisted of 2 μL cDNA, 1 μL of forward primer (10 μmol/L), 1 μL of reverse primer (10 μmol/L), 10 μL of 2× Master Mix, and 6 μL of RNase-free water. First, the reaction was denatured at 95 °C for 10 min, followed by 45 amplification cycles at 95 °C for 10 s, 60 °C for 60 s, and 95 °C for 15 s. After that, the relative expression levels of tsRNA were calculated using the $2^{-\triangle\triangle Ct}$ method and then normalized to the U6 expression levels. Finally, all the reactions were repeated in triplicate.

Cell lines and cell culture

Two cell lines, C666-1 with EBV and HNE1 without, were used for transient transfection, followed by experiments. The human NPC cell line C666-1 was purchased from the Abiowell company (AW-CCH168, China), and HNE1 was purchased from the BDBIO company (C6105, China). The STR reports of C666-1 and HNE1 cells were presented in Supplementary File 2 and Supplementary File 3. C666-1 and HNE1 cells were cultivated in RPMI Medium 1640 basic (1X) (6124417, Gibco, USA), which was supplemented with 10% fetal bovine serum (FBS) (2422322, VivaCell Biosciences, Shanghai, China) and 100 μg/mL of penicillin and streptomycin (01X240627, Abiowell, China), within an environment containing 5% CO_2.

Transient transfection

Between 1×10^6 and 5×10^6 cells were inoculated into 6-well plates containing an appropriate amount of complete culture medium, aiming to achieve a cell density of 50%–60% during transfection. Take two 1.5 mL EP tubes, labeled A tube and B tube, and add 250 μL Opti MEM (Gibco, USA) to each EP tube. Add 10 μL Lipofectamine 3000 (2773051, Invitrogen, USA) to A tube and 100 μmol/L 5′tiRNA-32-ValAAC-2 mimics (347RBE03, Accurate Biology, China) or 5′tiRNA-32-ValAAC-2 inhibitor (347RBE04, Accurate Biology, China) to B tube. Let the contents in tubes A and B stand for 5 min. Then, vortex and mix tubes A and B. Let the mixture stand for 20 min. Finally, add the AB mixture to 1.5mL serum-free culture medium. Discard the waste liquid from the 6-well plate, and then add 6 mL of the transfection solution to each well. After culturing in a CO_2 incubator at 37°C for 4–6 h, replace it with complete medium and continue culturing for 48 h before performing subsequent relevant experiments. The 5′tiRNA-32-ValAAC-2 mimics indicates overexpression of 5′tiRNA-32-ValAAC-2, and the 5′tiRNA-32-ValAAC-2 inhibitor inhibits the expression of 5′tiRNA-32-ValAAC-2. The NC group represent control group.

Cell viability assay

The viability of NPC cells was quantified by employing the Cell Counting Kit-8 (CCK-8) (Bs350A, Biosharp, Anhui, China) in strict accordance with the manufacturer's instructions. First, NPC cells (1×10^4/well) were inoculated into 96-well plates and grown to 60%–75% confluence. Then, 10 μL of Cell Counting

Kit-8 reagent was added, and the cells were incubated for 2 h at 37 °C. The absorbance was measured with a microplate reader (Thermo Scientific, USA) at 450 nm. Thereafter, the optical density (OD) values were measured at 2, 6, 12, 18, 24 and 30 h.

Colony growth assay

NPC cells were plated at a density of 300–500 cells per well in 6-well plates and then cultured in a cell incubator at 37 °C and 5% CO_2 for 10–14 d. The cells were fixed with methanol for 15 min. Then 0.1% crystal violet dye was added for 1–3 min, followed by a gentle rinse with running water. After being air-dried, the clone formation rate was calculated using the formula: clone formation rate = (number of clones/number of inoculated cells) × 100%.

Wound healing assay

NPC cells were seeded in 6-well plates at a density of 5×10^5 cells/well and cultured overnight. Scratches were created using a 200-μL pipette tip. Images were acquired at 0, 12, and 24 h using a microscope (Olympus, Japan). Gap distances were measured using ImageJ software.

Transwell cell migration assay

Cell migration assays were carried out using Transwell chambers according to the manufacturer's guidelines (02722042, Corning Costar, USA). NPC cells were plated in the upper Transwell chamber at a density of 4×10^4 cells per well, with 200 μL serum-free RPMI 1640 medium in the upper chamber and 800 μL complete culture medium in the lower chamber. The chambers were then incubated at 37 °C with 5% CO_2 for 24, 48, and 72 h. Then, the cells were fixed with 500 μL of 4% (w/v) paraformaldehyde solution and stained with 600 μL of 0.1% (w/v) crystal violet solution. Finally, the number of migrating cells was counted.

Transwell cell invasion assay

Cell invasion assays were performed in 24-well Transwell chambers with matrigel (3061003, Corning, USA). First, diluted matrigel was quickly spread into the upper chamber of the Transwell, and then the upper chamber was placed in a 37 °C incubator. The cell density was adjusted to 1×10^5–10×10^5 cells/mL and inoculated into the upper chambers. After 24, 48, and 72 h of cultivation, the cells were fixed in 4% (w/v) paraformaldehyde solution for 10 min, and then crystalline violet solution (0.1%, w/v) was added to the cell wells for 1–3 min. Images were acquired using an inverted microscope.

Statistical analysis

All data analyses were carried out using IBM SPSS Statistics 25.0 (IBM, Ehningen, Germany) and GraphPad Prism 9.5 (GraphPad Software, San Diego, CA, United States). The results of RT-qPCR were presented as the mean ± standard error of the mean (SEM). Unpaired *t*-tests were employed to compare the expression levels of each candidate tsRNA between NPC patients and normal individuals. Receiver operating characteristic (ROC) analysis was conducted in order to determine the diagnostic sensitivity and specificity of the tsRNA expression in serum. All experiments were repeated at least three times. *t*-tests were used to analyze differences between two groups, and the one-way ANOVA was utilized to analyze differences among three or more groups. Analysis items with $P < 0.05$ were considered statistically significant.

Results

Small RNA expression profiling of the serum from NPC patients and normal individuals

Serum samples from 20 NPC patients and 5 normal individuals were subjected to tsRNA sequencing [41–43]. The sequencing quality data are presented in Table S2. In this study, when comparing NPC patients with the control group, the age and gender of the two groups were basically matched, and this matching principle was applied in data analysis. The baseline characteristics of normal individuals are as follows: Among the 5 normal individuals, there were 4 males and 1 female. Regarding age distribution, 1 individual was aged 30–40 years, 1 individual was aged 41–50 years, 2 individuals were aged 51–60 years, and 1 individual was aged 61–70 years. The baseline characteristics of NPC patients are summarized in Table 1. Among the 20 NPC patients, there were 14 males and 6 females. Regarding age distribution, 2 patients were aged 30–40 years, 6 patients were aged 41–50 years, 8 patients were aged 51–60 years, and 4 patients were aged 61–70 years. The frequency ratios of gender and the individual quantifications of age are matched between the NPC patients and normal individuals mentioned above. In addition, 80% of NPC patients had non-keratinous carcinoma of undifferentiated histology type. In terms of pathological stage, 5 patients were at stage II, 4 patients were at stage III, 11 patients were at stage IV. The elevated expression of Ki-67 in immunohistochemistry serves as a characteristic sign of cancer advancement. The higher the expression level of Ki-67, and the higher the proportion of cells in the division stage [44], and the faster the tumor growth [45], and the later the stage [46], and the higher the probability of gene mutation and drug resistance mutation [47], and

the higher the tumor mutation load [48,49]. In NPC patients, Ki-67 levels between 10% and 50% indicate low tumor proliferation, whereas Ki-67 levels > 50%, showing markedly increased proliferation [50], are an independent risk factor for cancer progression [51]. In this study, the number of patients with Ki-67 expression levels detected by immunohistochemistry is as follows: 12 patients had expression levels ranging from 10% to 50%, and 8 patients had expression levels > 50%.

To investigate comprehensively small RNA profiles, we analyzed the distribution of various types of small RNAs in serum, such as microRNA (miRNA), pre-miRNA, snoRNA, tRNA, and tRNA-derived small RNAs (tsRNA, or tRF and tiRNA). The results are shown in Fig. 2. As illustrated in Fig. 2A, the 5 parts of the small RNA biotypes in the sera were not significantly different between NPC patients and normal individuals ($P = 0.313$ of miRNA, $P = 0.736$ of pre-miRNA, $P = 0.655$ of snoRNA, $P = 0.635$ of tRNA, $P = 0.391$ of tsRNA). tsRNA accounted for the largest proportion of small RNA, reaching 40.21% in NPC patients (Fig. 2B) and 40.28% in normal individuals (Fig. 2C). A total of 7 types of tsRNAs were identified in 2 groups, including 5′tRF, 3′tRF, tRF-1, 5-Leader, 5′tiRNA, 3′tiRNA, and i-tRF. Fig. 2D and 2E present the percentage of expression with various tsRNA subtypes. Comparing NPC patients and normal individuals, the proportions of 5′tRF are 38.97% and 38.50% respectively; for 5′tiRNA, they are 17.53% and 17.45%; for 3′tRF, 15.52% and 15.81%; for i-tRF, 13.40% and 13.24%; for 5-Leader, 8.24% and 8.45%; for 3′tiRNA, 3.71% and 3.87%; and for tRF-1, 2.63% and 2.68%. 5′tRF is the most abundant tsRNA in the sera, followed by 5′tiRNA, 3′tRF, i-tRF, 5-Leader, 3′tiRNA, and tRF-1 (Fig. 2F). From the above research results, we can conclude that tsRNA is the most highly expressed among the distribution of small RNAs in both NPC patients and normal individuals. To screen for a biomarker for NPC diagnosis, highly-expressed tsRNA was selected for subsequent experiments.

Expression spectrums of tsRNAs in serum from NPC patients and normal individuals

The RNA sequencing results indicated that a total of 3738 tsRNAs were detected in the array sequencing. Among these, 549 tsRNAs were not included by the MINTbase. There were 132 functional tsRNAs, 670 reliable tsRNAs, and 2936 potential tsRNAs. Specifically, researchers documented the functional tsRNAs with characterized biological functions or disease association; the reliable tsRNAs were recorded in tRFdb or reported in literature but lacked in-deepth research; the potential tsRNAs were computationally predicted by Arraystar based on the lengths of RNA fragments and the cleavage positions in the tRNA. The main types of functional tsRNAs were 5′tiRNA and tRF-1. In the reliable tsRNAs, i-tRF, tRF-1, and 5′tRF were predominantly detected. And within the potential tsRNAs, a large quantity of 5′tRF, 3′tRF, and 5′tiRNA were found (Fig. 3A–3C). The principal component analysis (PCA) plot to visualize the overall expression profile differences of tsRNAs between NPC patients and normal individuals. In Fig. 4A, the normal individuals were distributed in the middle and relatively scattered, indicating significant sample differences in the NC group. In contrast, the NPC group was mainly concentrated in the middle and more densely distributed, indicating small sample differences in the experimental group. Overall, both sets of samples are highly representative and meet the testing criteria. To further analyze the differentially expressed tsRNAs between NPC patients and normal individuals, a hierarchical clustering heat-map was employed to visualize the expression spectrum of tsRNAs in Fig. 4B. Compared with the normal individuals, 42 tsRNAs were upregulated, and 48 tsRNAs were downregulated in NPC patients (Fig. 4C). Furthermore, when $P < 0.05$, tsRNAs were considered to have significantly differential expressions. From the volcano plot in Fig. 4D, 9 upregulated tsRNAs and 11 downregulated tsRNAs were identified. The 9 upregulated tsRNAs with FC > 1.5, regarded as the most significantly potential tsRNAs, were applied to the subsequent experimental validation.

Differentially expressed specific tsRNAs in primary diagnosed NPC patients

Based on the criteria of FC > 1.5 and $P < 0.05$, 9 upregulated tsRNAs were identified as candidate tsRNAs (Table 2). Subsequently, to further investigate these candidate tsRNAs, the expression levels of these candidate tsRNAs were validated in serum samples from two groups using RT-qPCR (20 serum samples from NPC patients and 5 from normal individuals). When compared to the control group, 5′tiRNA-32-ValAAC-2, tRF5-50-GlyGCC-2, i-tRF-4:24-His-GTG-1, i-tRF-2:25-His-GTG-1, tRF5-31-HisGTG-1, tRF5-23-HisGTG-1, 5′tiRNA-34-GlnTTG-6, and mt-tRF5-26-LeuTAA were all statistically upregulated in the NPC group. In contrast, 5′tiRNA-35-GlnTTG-6 had not been significantly expressed (Fig. 5). These results are consistent with tsRNA sequencing data. Compared with the control group, the 8 potential tsRNAs were upregulated in patients with newly diagnosed NPC. tRF5-50-GlyGCC-2 was highly expressed with P-value < 0.05. i-tRF-4:24-His-GTG-1, i-tRF-2:25-His-GTG-1, tRF5-31-HisGTG-1, and mt-tRF5-26-LeuTAA were also highly expressed with $P < 0.01$. 5′tiRNA-34-GlnTTG-6 was highly expressed with $P < 0.001$. 5′tiRNA-32-ValAAC-2 and tRF5-23-HisGTG-1 were the most significantly expressed with $P < 0.0001$.

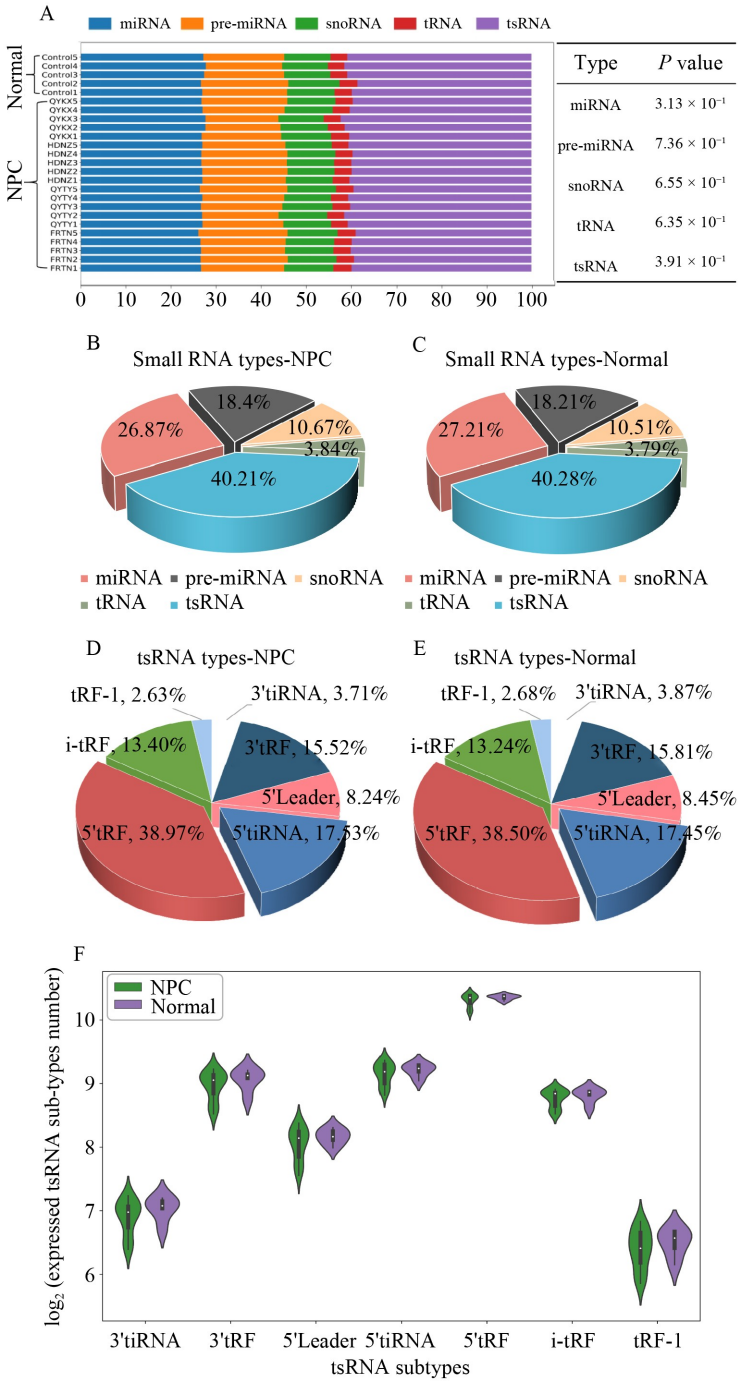

Fig. 2 Distribution of small RNAs and tsRNA types in NPC patients' serum. (A) Small RNA distribution in the sera from NPC patients or normal individuals, the right panel displays *P* value of the difference between normal and NPC samples. The percentage of small RNA types in the sera from (B) NPC patients and (C) normalindividuals using pie chart. The percentage of tsRNA types in the sera of (D) NPC patients and (E) normalindividuals using pie chart. (F) The expressed numbers of tsRNA types in the sera from normal individuals and NPC patients using violin plot.

Potential value of the validated tsRNA in NPC diagnosis

To evaluate the diagnostic value of the 9 tsRNAs, the serum tsRNAs of newly diagnosed NPC patients were assessed using ROC curves. Table 3 and Fig. 6 show the AUC, sensitivity, and specificity of 5′tiRNA-32-ValAAC-2, tRF5-50-GlyGCC-2, i-tRF-4:24-His-GTG-1, i-tRF-2:25-His-GTG-1, 5′tiRNA-35-GlnTTG-6, tRF5-31-HisGTG-1, tRF5-23-HisGTG-1, 5′tiRNA-34-GlnTTG-6, and mt-tRF5-26-LeuTAA. tRF5-23-HisGTG-1 (AUC = 1.000, Sensitivity = 100%, Specificity = 100%), 5′tiRNA-

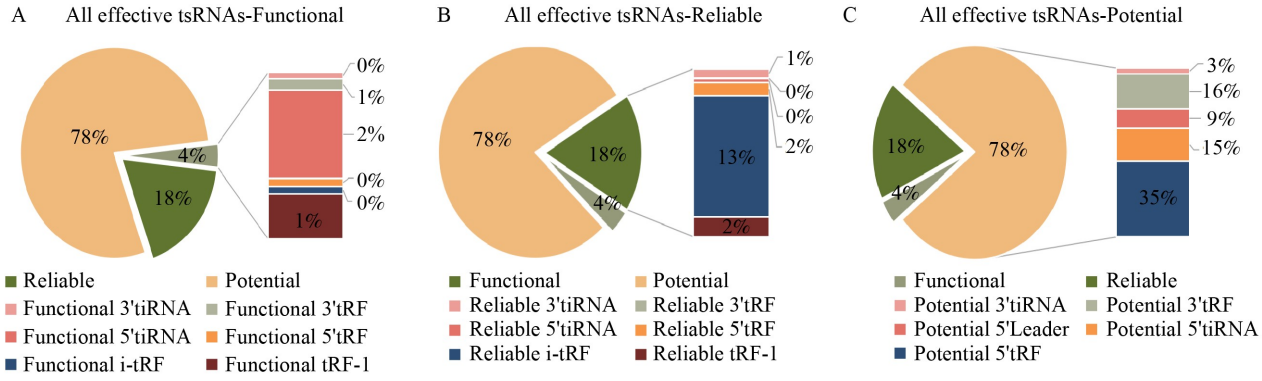

Fig. 3 Three tsRNA types in NPC patients' serum. (A) Percentage of functional tsRNA types of NPC patients using composite pie chart. (B) Percentage of reliable tsRNA types of NPC patients using composite pie chart. (C) Percentage of potential tsRNA types of NPC patients using composite pie chart.

32-ValAAC-2 (AUC = 0.960, Sensitivity = 85%, Specificity = 95%), tRF5-31-HisGTG-1 (AUC = 0.953, Sensitivity = 85%, Specificity = 90%), i-tRF-2:25-His-GTG-1 (AUC = 0.950, Sensitivity = 95%, Specificity = 100%), and 5′tiRNA-34-GlnTTG-6 (AUC = 0.915, Sensitivity = 100%, Specificity = 75%) may serve as potential diagnostic biomarkers for initially diagnosed NPC. The AUC values of the remaining 4 tsRNAs are less than 0.900 (tRF5-50-GlyGCC-2, i-tRF-4:24-His-GTG-1, 5′tiRNA-35-GlnTTG-6, and mt-tRF5-26-LeuTAA). The complete statistical analysis is presented in Table S3.

Specific value of 5′tiRNA-32-ValAAC-2 in NPC diagnosis

According to the AUC value and previous PCR results, 5′tiRNA-32-ValAAC-2 was chosen for further investigation. We used RT-qPCR to further validate 5′tiRNA-32-ValAAC-2 expression in two groups (100 NPC patients vs. 20 normal individuals) during the testing phases. The results indicated that the level of 5′tiRNA-32-ValAAC-2 in NPC patients was higher than that in normal individuals (Fig. 7A and 7B, $P < 0.05$). In the ROC curve, 5′tiRNA-32-ValAAC-2 demonstrated statistical significance $P < 0.001$, with an AUC = 0.994, 93% sensitivity, 100% specificity, and 95% CI ranging from 0.984 to 1.000 (Fig. 7C). The clinical data along with baseline characteristics of 100 NPC patients are presented in Table S4.

The main gene network relationships of 5′tiRNA-32-ValAAC-2 are shown in Fig. 8A. Meanwhile, the positions of 5′tiRNA-32-ValAAC-2 on the cloverleaf secondary structure are shown in Fig. 8B. TargetScan and miRanda were used to construct the tsRNA and target gene network of initially diagnosed NPC. When the context score was ⩽ −0.2, 5′tiRNA-32-ValAAC-2 has 199 candidate target genes. The top 5 genes of 5′tiRNA-32-ValAAC-2 are presented in Table 4. *UGT2B7*, *SYNPO2*, *ZNF44*, *PDHB*, and *UFM1* associated with 5′tiRNA-32-ValAAC-2 have a context score < −0.5 (Fig. 8C). In Table 4, the context score of *UGT2B7* is −0.576, with 178 structure score and −27.75 energy score; the context score of *SYNPO2* is −0.529, with 162 structure score and −21.16 energy score; the context score of *ZNF44* is −0.524, with 167 structure score and −23.78 energy score; the context score of *PDHB* is −0.513, with 172 structure score and −22.9 energy score; the context score of *UFM1* is −0.505, with 167 structure score and −24.82 energy score. *UGT2B7*, *SYNPO2*, *ZNF44*, and *UFM1* all promote tumor migration and invasion, while *PDHB* inhibits tumor proliferation, migration, and invasion.

5′tiRNA-32-ValAAC-2 regulates the expression of NPC cells with RT-qPCR

To ascertain the role of 5′tiRNA-32-ValAAC-2 in NPC cells (C666-1 and HNE1), the expression of 5′tiRNA-32-ValAAC-2 was induced using mimics. Then, RT-qPCR was performed to measure 5′tiRNA-32-ValAAC-2 expression levels (Fig. 9A). Compared to the NC group, the expression of 5′tiRNA-32-ValAAC-2 in mimics group was markedly higher in the C666-1 ($P = 0.0039$) and HNE1 ($P = 0.0005$) cells. Conversely, the expression of 5′tiRNA-32-ValAAC-2 in NPC cells (C666-1 and HNE1) was reduced by the inhibitor. RT-qPCR showed that, compared to the NC group, the expression of 5′tiRNA-32-ValAAC-2 in inhibitor group was significantly lower in the C666-1 ($P = 0.0119$) and HNE1 ($P = 0.0006$) cells (Fig. 10A). The results proved that 5′tiRNA-32-ValAAC-2 was exactly highly expressed in NPC.

5′tiRNA-32-ValAAC-2 regulates the proliferation of NPC cells with CCK-8 assay and colony growth assay

The viability of both C666-1 and HNE1 cell lines that

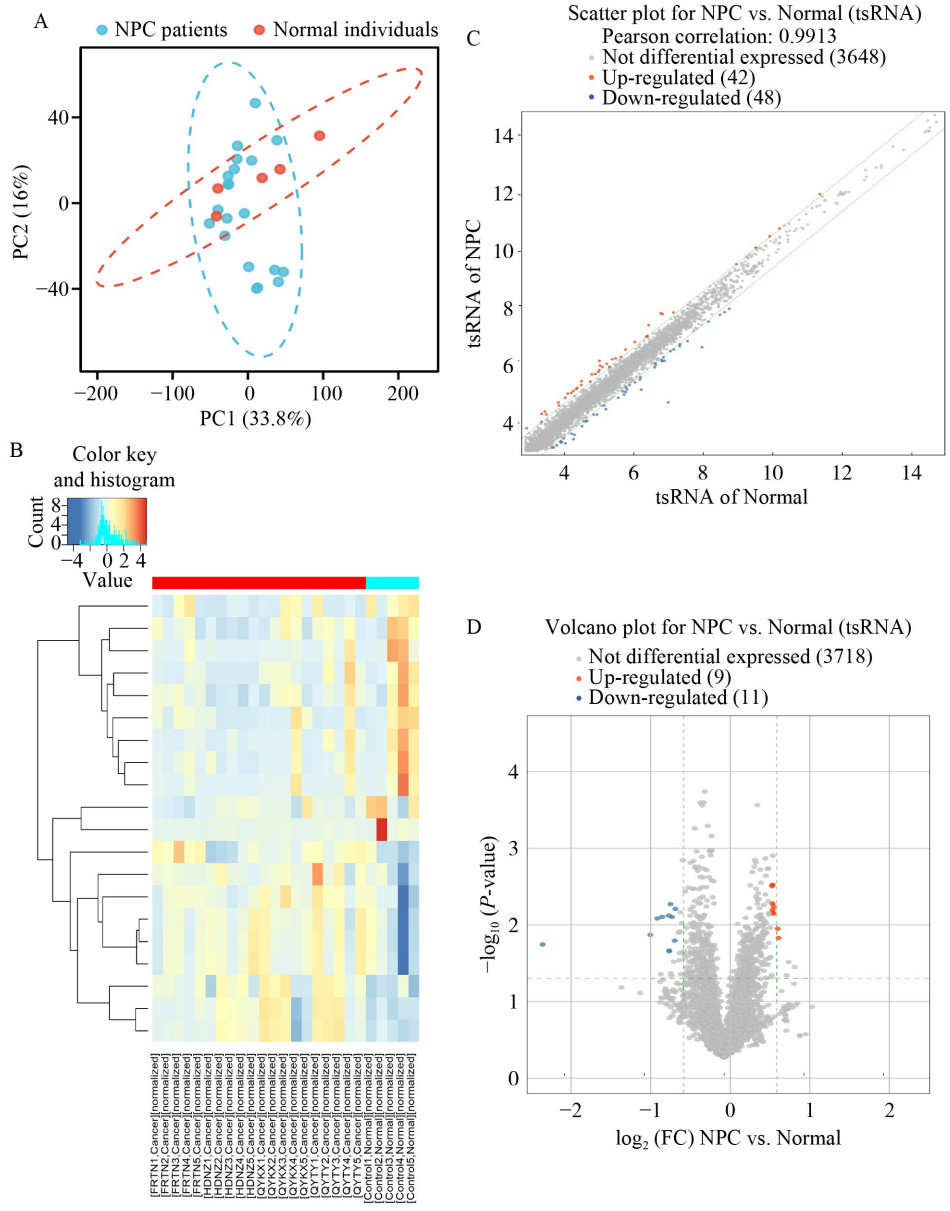

Fig. 4 Analysis of differentially expressed tsRNAs in NPC patients' serum. (A) The PCA plot of tsRNAs between NPC patients and normal individuals. (B) Hierarchical clustering heatmap for the tsRNAs. The color in the panel represents the relative expression level (log_2-transformed), blue represents an expression level below the mean, and red represents an expression level above the mean. (C) Scatter plots of differentially expressed tsRNAs. tsRNAs above the top line (red dots, upregulation) or below the bottom line (blue dots, downregulation) show more than 1.5-fold change between the two compared groups. (D) Volcano plots of significantly differentially expressed tsRNAs. The values of the X axis in the volcano plot were log_2-transformed fold change and Y axis with $-log_{10}$-transformed *P*-values between the two groups. Red/blue circles indicate statistically significant differentially expressed tsRNAs with a FC of no less than 1.5 and a $P < 0.05$ (red, upregulated; blue, downregulated).

were transfected with or without 5′tiRNA-32-ValAAC-2 mimics was evaluated through the CCK-8 assay. The results indicated that, when compared with the control group, C666-1 and HNE1 cells transfected with the mimics both exhibited high viability levels (Fig. 9B). In C666-1 cells, the mimics group compared with NC group were $P = 0.0025$ at 2 h, $P = 0.0087$ at 6 h, $P = 0.0144$ at 12 h, $P = 0.0012$ at 18 h, $P = 0.0012$ at 24 h, $P = 0.0397$ at 30 h. And in HNE1 cells, the mimics group compared with NC group were $P = 0.0179$ at 2 h, $P = 0.0108$ at 6 h, $P < 0.0001$ at 12 h, $P < 0.0001$ at 18 h, $P < 0.0001$ at 24 h, $P = 0.0001$ at 30 h. On the other hand, when the expression of 5′tiRNA-32-ValAAC-2 was inhibited in C666-1 and HNE1 cells, the viability levels were lower compared to those in the control group cells (Fig. 10B). In C666-1 cells, the *P*-values for 5′tiRNA-32-ValAAC-2 inhibitor group versus NC group were 0.0010 at 2 h, 0.0091 at 6 h, 0.0092 at 12 h, 0.0161 at 18 h, 0.0123 at

Table 2 Sequencing information of upregulated potential tsRNAs

tsRNA ID	Fold change	*P*-value	tsRNA type	tsRNA-sequence	tsRNA-length
5′tiRNA-32-ValAAC-2	1.606	0.028	5′tiRNA	GTTTCCGTAGTGTAGTGGTCATCACGTTCGCC	32
tRF5-50-GlyGCC-2	1.594	0.021	5′tRF	GCATTGGTGGTTCAGTGGTAGAATTCTCGCCTGCC ACGCGGGAGGCCCGG	50
i-tRF-4:24-His-GTG-1	1.540	0.011	i-tRF	GTGATCGTATAGTGGTTAGTA	21
i-tRF-2:25-His-GTG-1	1.537	0.013	i-tRF	CCGTGATCGTATAGTGGTTAGTAC	24
5′tiRNA-35-GlnTTG-6	1.523	0.012	5′tiRNA	GACCATGTGGCCTAAGGGAAAAGACATCTCACTTT	35
tRF5-31-HisGTG-1	1.523	0.006	5′tRF	GCCGTGATCGTATAGTGGTTAGTACTCTGCG	31
tRF5-23-HisGTG-1	1.522	0.013	5′tRF	GCCGTGATCGTATAGTGGTTAGT	23
5′tiRNA-34-GlnTTG-6	1.520	0.010	5′tiRNA	GACCATGTGGCCTAAGGGAAAAGACATCTCACTT	34
mt-tRF5-26-LeuTAA	1.517	0.006	5′tRF	GTTAAGATGGCAGAGCCCGGTAATCG	26

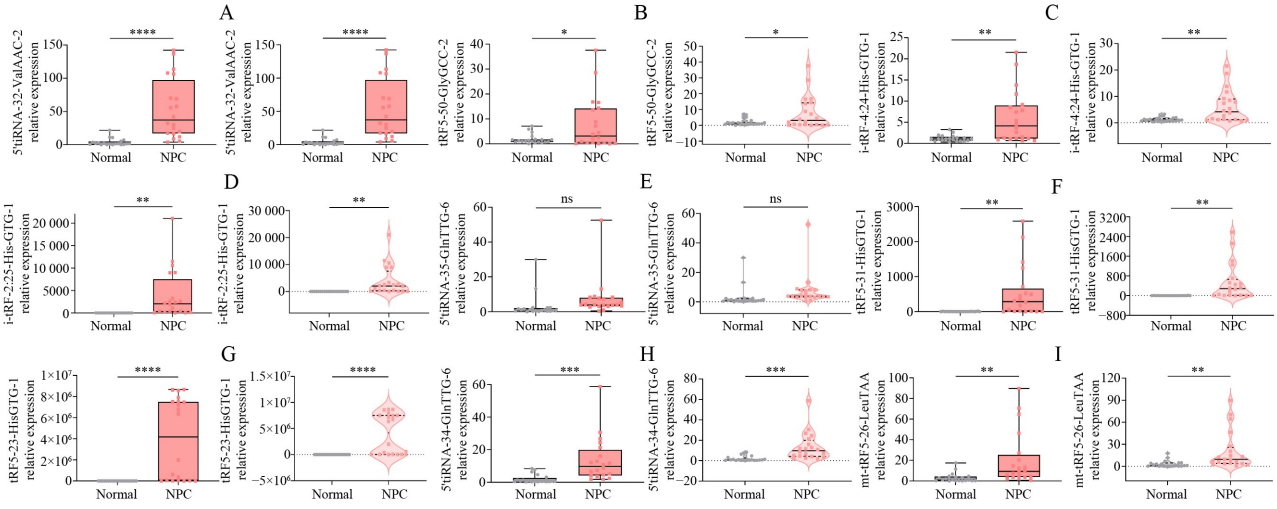

Fig. 5 Verification of the upregulated tsRNAs expression in serum from NPC patients and normal individuals by RT-qPCR. (A) 5′tiRNA-32-ValAAC-2. (B) tRF5-50-GlyGCC-2. (C) i-tRF-4:24-His-GTG-1. (D) i-tRF-2:25-His-GTG-1. (E) 5′tiRNA-35-GlnTTG-6. (F) tRF5-31-HisGTG-1. (G) tRF5-23-HisGTG-1. (H) 5′tiRNA-34-GlnTTG-6. (I) mt-tRF5-26-LeuTAA. *$P < 0.05$, **$P < 0.01$, ***$P < 0.001$, ****$P < 0.0001$. ns, non-significant.

Table 3 ROC analysis of the specific validated tsRNAs.

tsRNA ID	AUC	Stand error	*P* value (area = 0.5)	95% CI	Sensitivity	Specificity
5′tiRNA-32-ValAAC-2	0.960	0.028	0.000***	0.908–1.000	85%	95%
tRF5-50-GlyGCC-2	0.609	0.098	0.239	0.416–0.801	60%	80%
i-tRF-4:24-His-GTG-1	0.800	0.070	0.001**	0.662–0.938	60%	95%
i-tRF-2:25-His-GTG-1	0.950	0.049	0.000***	0.854–1.000	95%	100%
5′tiRNA-35-GlnTTG-6	0.853	0.071	0.000***	0.713–0.992	90%	90%
tRF5-31-HisGTG-1	0.953	0.029	0.000***	0.895–1.000	85%	90%
tRF5-23-HisGTG-1	1.000	0.000	0.000***	1.000–1.000	100%	100%
5′tiRNA-34-GlnTTG-6	0.915	0.043	0.000***	0.830–1.000	100%	75%
mt-tRF5-26-LeuTAA	0.850	0.059	0.000***	0.733–0.967	95%	60%

**$P < 0.01$, ***$P < 0.001$.

24 h, 0.0011 at 30 h; and in HNE1 cells, they were 0.0233 at 2 h, < 0.0001 at 6 h, 0.0002 at 12 h, 0.0412 at 18 h, 0.0002 at 24 h, 0.0117 at 30 h. The results indicated that the inhibition of 5′tiRNA-32-ValAAC-2 exerted a suppressive effect on the proliferation of NPC cells. Therefore, these findings suggested that 5′tiRNA-32-

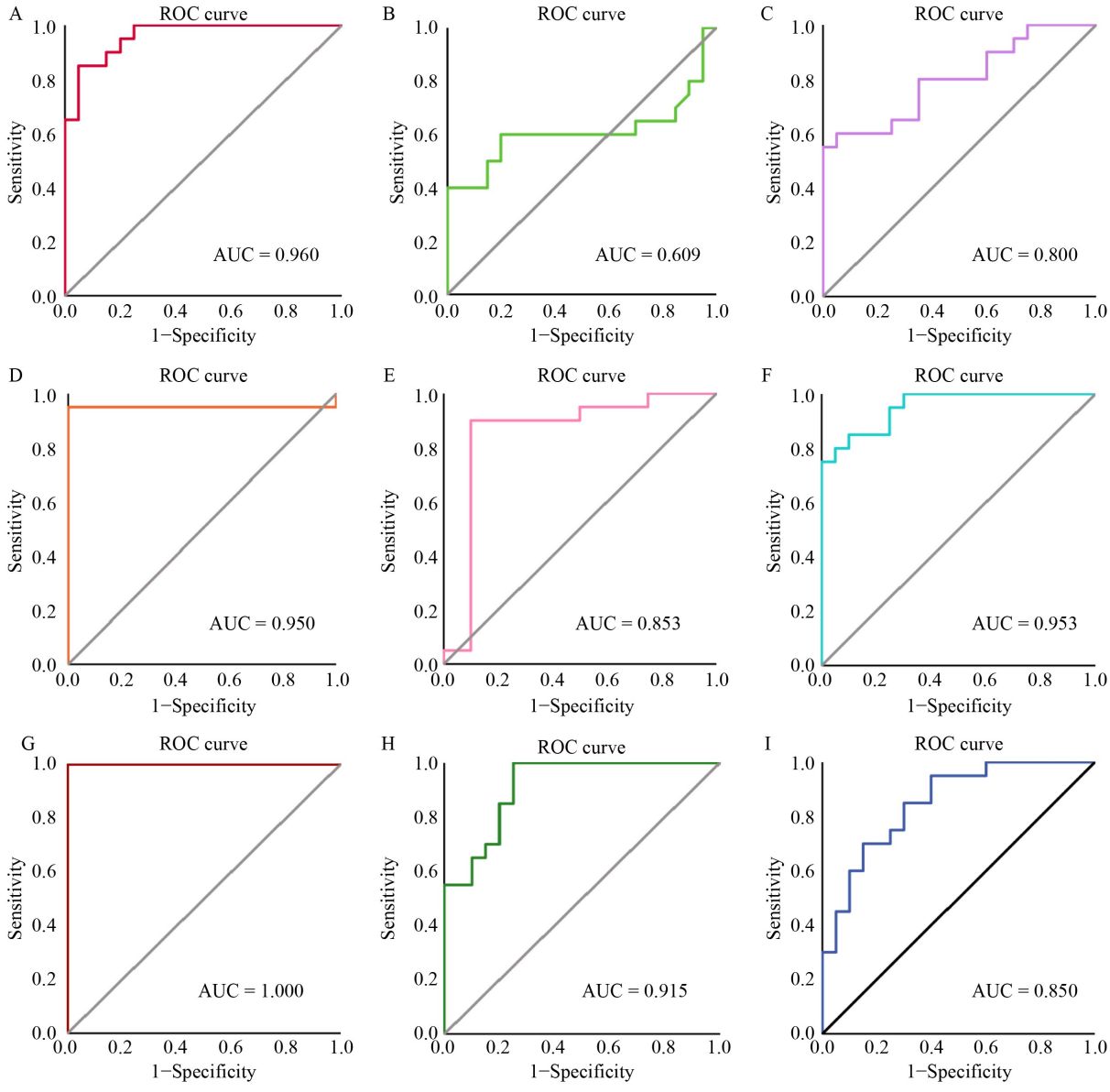

Fig. 6 ROC analysis of newly diagnosed NPC prediction based on the specific tsRNAs. (A) 5′tiRNA-32-ValAAC-2. (B) tRF5-50-GlyGCC-2. (C) i-tRF-4:24-His-GTG-1. (D) i-tRF-2:25-His-GTG-1. (E) 5′tiRNA-35-GlnTTG-6. (F) tRF5-31-HisGTG-1. (G) tRF5-23-HisGTG-1. (H) 5′tiRNA-34-GlnTTG-6. (I) mt-tRF5-26-LeuTAA.

ValAAC-2 played a stimulatory role in the proliferation of NPC cells.

In C666-1 cells, the clone formation numbers of NPC cells with the mimics group and NC group were 169.70 and 49.00, respectively ($P < 0.0001$). And in HNE1 cells, the numbers were 273.3 and 82.33 ($P = 0.0006$) (Fig. 9C). Conversely, the clone formation numbers of the NPC cells with the inhibitor group versus NC group were 91.67 and 297.30 in C666-1 cells ($P = 0.0482$), and 93.00 and 256.30 in HNE1 cells ($P = 0.0016$), respectively (Fig. 10C). These results indicated that 5′tiRNA-32-ValAAC-2 had a promoting effect on colony-forming ability of NPC cells.

5′tiRNA-32-ValAAC-2 regulates the migration of NPC cells with scratch assay and Transwell cell migration assay

In addition, the scratch assay demonstrated that overexpression of 5′tiRNA-32-ValAAC-2 enhanced the motility of C666-1 and HNE1 cells (Fig. 9D). Compared with the NC group, the wound areas of the mimics group were smaller in C666-1 cells ($P < 0.0001$ at 24 h, $P = 0.0137$ at 48 h) and HNE1 cells ($P = 0.0017$ at 24 h, $P = 0.0332$ at 48 h). Moreover, the scratch assay (Fig. 10D) confirmed that inhibition of 5′tiRNA-32-ValAAC-2 restrained the motility of C666-1 and HNE1 cells. The

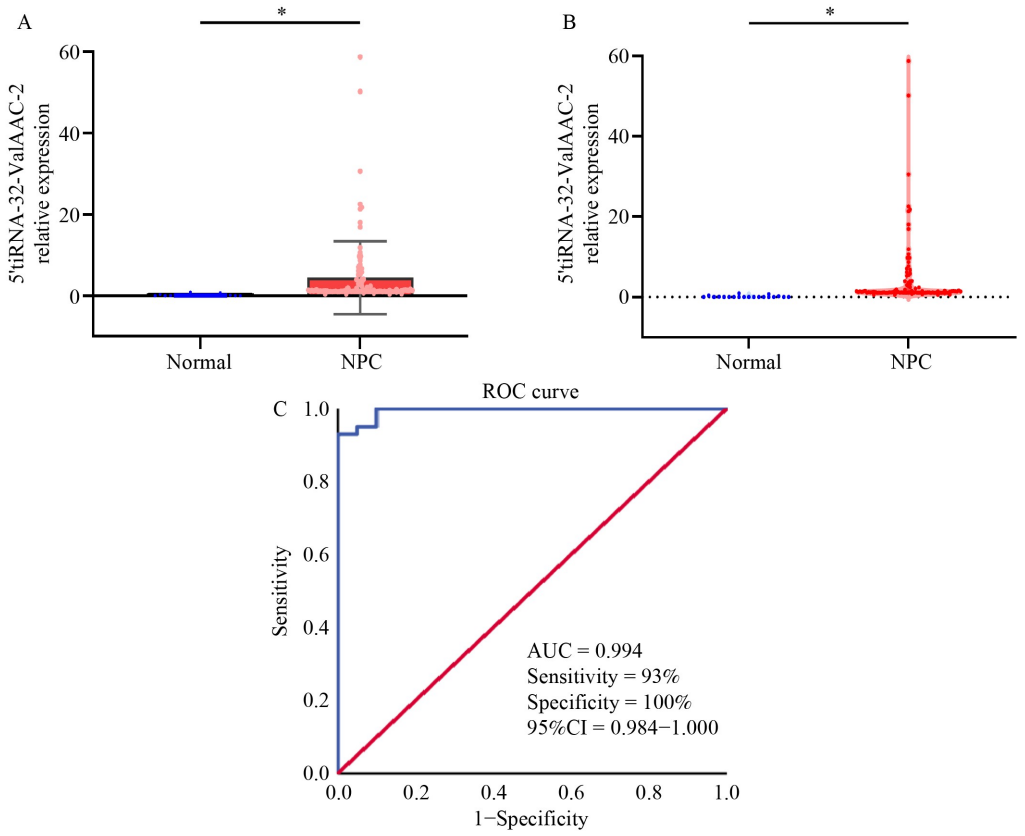

Fig. 7 Specific values of 5′tiRNA-32-ValAAC-2 in newly diagnosed NPC. Verification of 5′tiRNA-32-ValAAC-2 expression levels in the sera from newly diagnosed NPC patients and normal individuals by RT-qPCR in (A) histogram and (B) violin chart. (C) ROC analysis of 5′tiRNA-32-ValAAC-2 in newly diagnosed NPC.

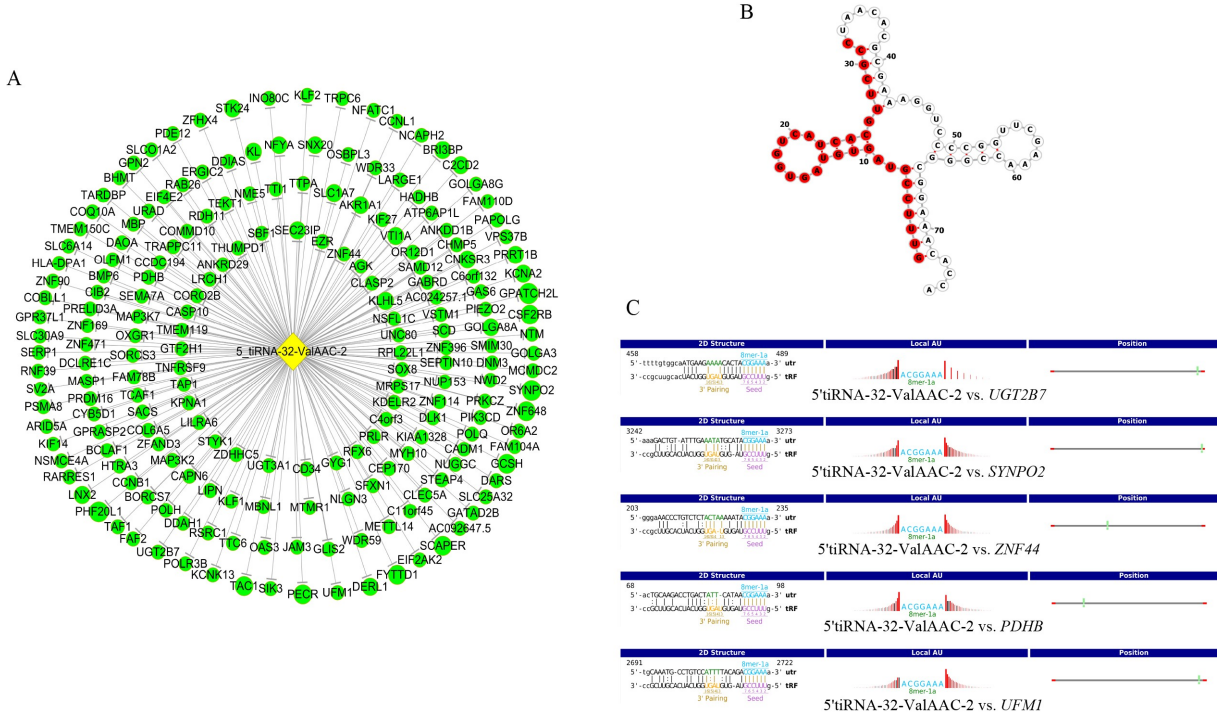

Fig. 8 5′tiRNA-32-ValAAC-2 structure and its associated genes. (A) 5′tiRNA-32-ValAAC-2 network diagram. (B) 2D Structure of 5′tiRNA-32-ValAAC-2. (C) Target gene sites for 5′tiRNA-32-ValAAC-2.

Table 4 Information of 5′tiRNA-32-ValAAC-2-gene in newly diagnosed NPC

mRNA	Context	Structure	Energy	Seed match types	Function
UGT2B7	−0.576	178	−27.75	8mer-1a	Promotes tumor migration and invasion [52], N6-methyladenosine (m^6A) modification [53]
SYNPO2	−0.529	162	−21.16	8mer-1a	Promotes tumor invasion and migration [54,55]
ZNF44	−0.524	167	−23.78	8mer-1a	Promotes tumor invasion [56]
PDHB	−0.513	172	−22.9	8mer-1a	Inhibits tumor proliferation, migration, and invasion [57,58]
UFM1	−0.505	167	−24.82	8mer-1a	Promotes tumor proliferation, migration, and invasion [59,60]

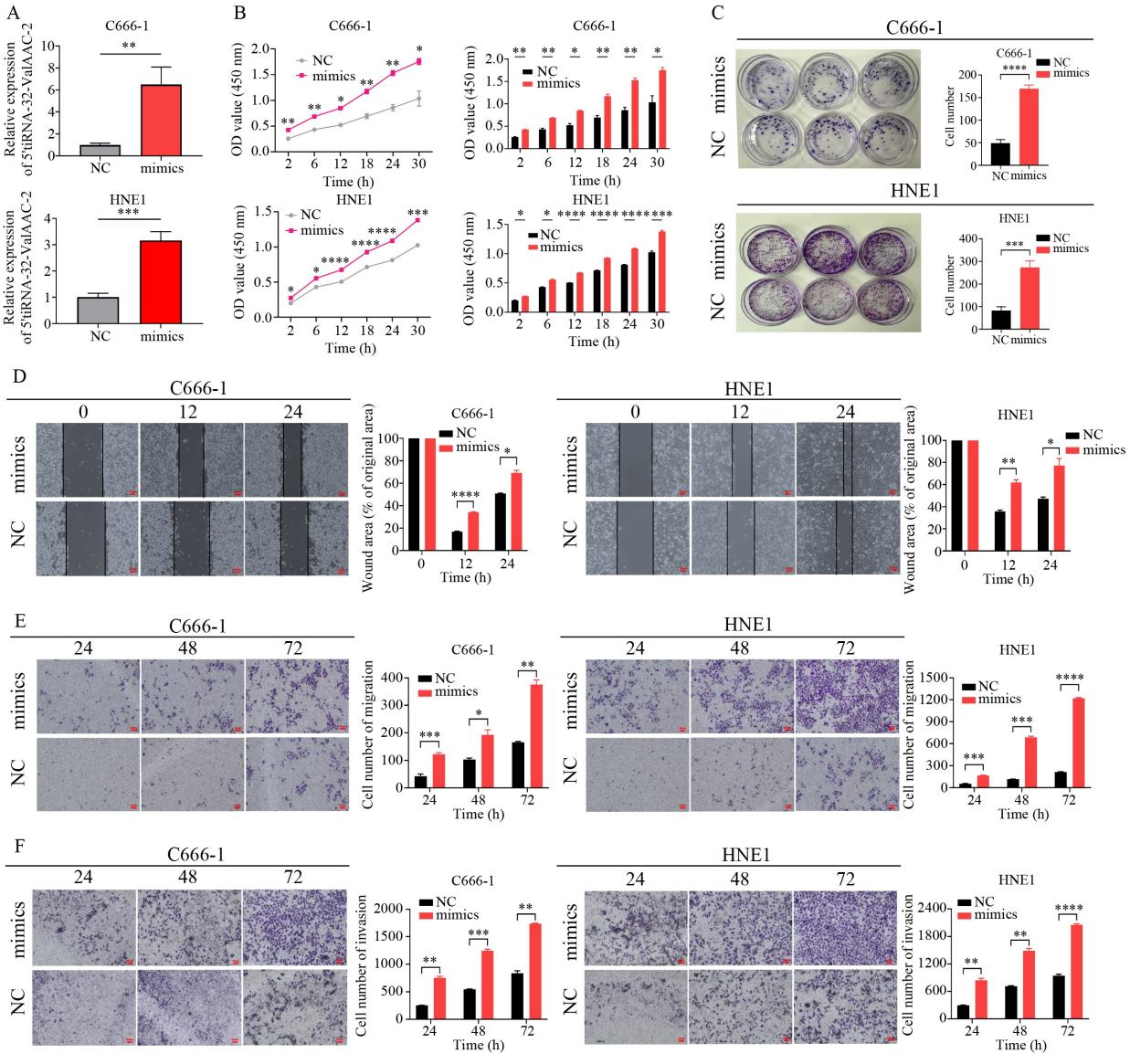

Fig. 9 5′tiRNA-32-ValAAC-2 promotes NPC cells proliferation, migration and invasion. (A) RT-qPCR. (B) Cell proliferation was detected by CCK-8 assay. (C) Cell proliferation was detected by clone formation assay. (D) Cell migration was detected by wound healing assay. (E) Cell migration was detected by Transwell assay. (F) Cell invasion was detected by Transwell assay. *$P < 0.05$, **$P < 0.01$, ***$P < 0.001$, ****$P < 0.0001$.

comparison of the wound areas between the 5′tiRNA-32-ValAAC-2 inhibitor group and NC group revealed that in C666-1 cells, $P = 0.0181$ at 24 h, $P < 0.0001$ at 48 h; in HNE1 cells, $P = 0.0017$ at 24 h, $P = 0.0002$ at 48 h. These results imply that 5′tiRNA-32-ValAAC-2 promotes the migratory capacity of NPC cells.

The Transwell cell migration assay (Fig. 9E) displayed that overexpression of 5′tiRNA-32-ValAAC-2 increased

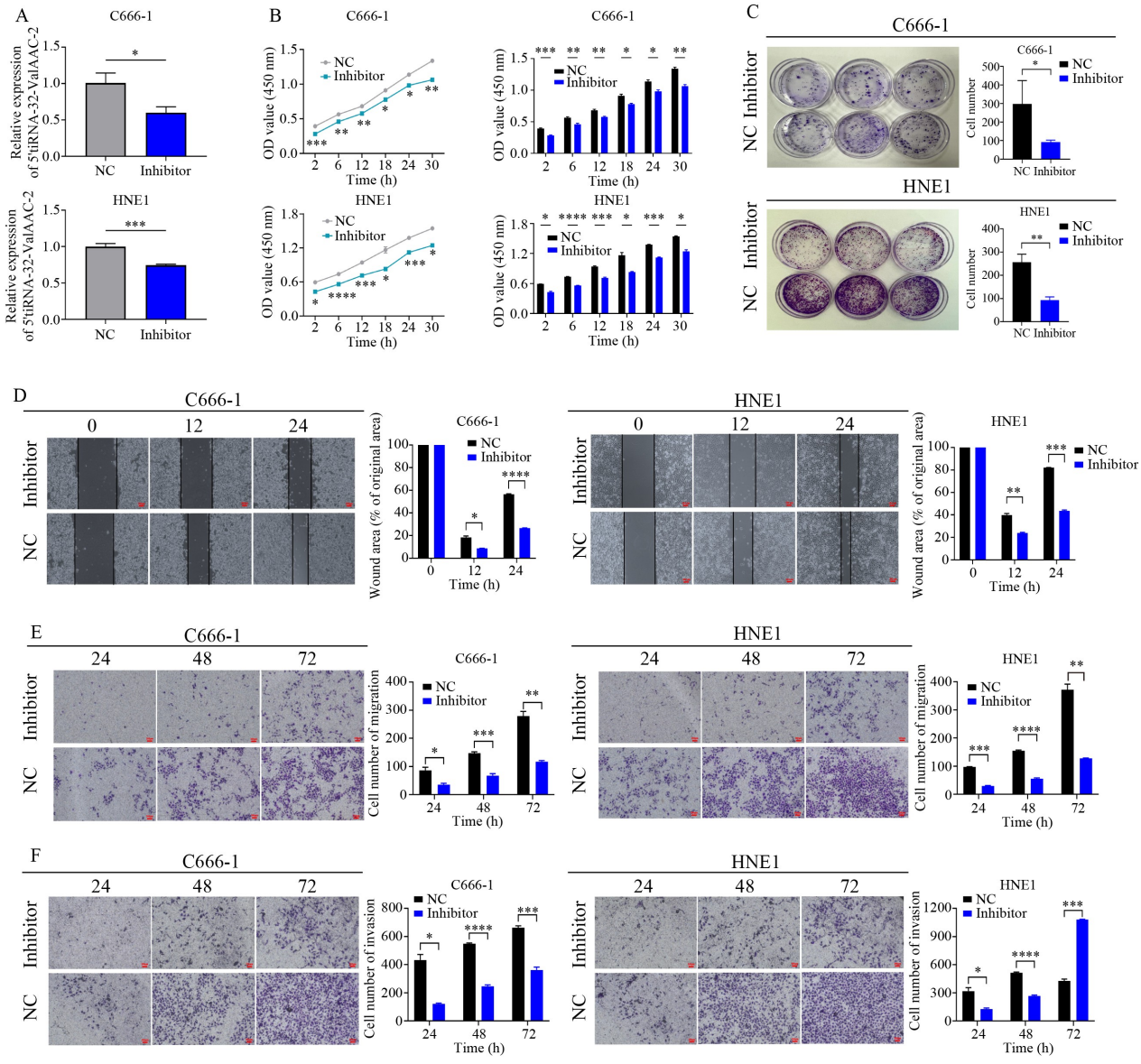

Fig. 10 5′tiRNA-32-ValAAC-2 inhibition decreases NPC cells proliferation, migration and invasion. (A) RT-qPCR. (B) Cell proliferation was detected by CCK-8 assay. (C) Cell proliferation was detected by clone formation assay. (D) Cell migration was detected by wound healing assay. (E) Cell migration was detected by Transwell assay. (F) Cell invasion was detected by Transwell assay. *$P < 0.05$, **$P < 0.01$, ***$P < 0.001$, ****$P < 0.0001$.

the migration ability of NPC cells. When comparing the mimics group with the NC group, in C666-1 cells, $P = 0.0008$ at 24 h, $P = 0.0211$ at 48 h, and $P = 0.0047$ at 72 h; and in HNE1 cells, the $P = 0.0010$ at 24 h, $P = 0.0005$ at 48 h, and $P < 0.0001$ at 72 h. On the other hand, the Transwell cell migration assay (Fig. 10E) verified that the inhibition of 5′tiRNA-32-ValAAC-2 diminished the migratory ability of NPC cells. When comparing the inhibitor group with NC group, in C666-1 cells, the $P = 0.0152$ at 24 h, $P = 0.0006$ at 48 h, and $P = 0.0077$ at 72 h; and in HNE1 cells, the $P = 0.0004$ at 24 h, $P < 0.0001$ at 48 h, and $P = 0.0062$ at 72 h. Therefore, as the above results indicate, 5′tiRNA-32-ValAAC-2 facilitates the migratory ability of NPC cells.

5′tiRNA-32-ValAAC-2 regulates the invasion of NPC cells with Transwell cell invasion assay

And the Transwell cell invasion assay (Fig. 9F) revealed that overexpression of 5′tiRNA-32-ValAAC-2 boosted the invasive ability of NPC cells. The comparison of the mimics group with NC group, the *P*-values were $P = 0.0022$ at 24 h, $P = 0.0006$ at 48 h, $P = 0.0015$ at 72 h in C666-1 cells; and $P = 0.0051$ at 24 h, $P = 0.0035$ at 48 h, $P < 0.0001$ at 72 h in HNE1 cells. Conversely, the Transwell cell invasion assay (Fig. 10F) verified that

inhibition of 5′tiRNA-32-ValAAC-2 reduced the invasive ability of NPC cells. The comparison of the inhibitor group with NC group, the *P*-values were $P = 0.0131$ at 24 h, $P < 0.0001$ at 48 h, $P = 0.0002$ at 72 h in C666-1 cells; and $P = 0.0228$ at 24 h, $P < 0.0001$ at 48 h, $P = 0.0003$ at 72 h in HNE1 cells. Based on the significant differences in the comparison between the experimental group and NC group, the above results demonstrate that 5′tiRNA-32-ValAAC-2 promotes the invasion ability of NPC cells.

Discussion

To screen an early-diagnosis marker for NPC, significant attention has been paid to small RNAs including miRNA, circRNA, particularly tsRNA. The roles and mechanisms of miRNA [61–63], lncRNA [64–66] and circRNA [67–69] in the development of NPC have been reported previously, yet they have not emerged as effective diagnostic markers. tsRNAs, as a class of small non-coding RNAs derived from tRNAs, are a newly discovered group of small non-coding RNAs generated from mature tRNA or tRNA precursors through cleavage by enzymes such as angiogenin, Dicer, RNase Z, and RNase P [70]. Through a variety of mechanisms, tsRNAs interact with proteins or mRNA, inhibit translation, and regulate gene expression, the cell cycle, chromatin status, and epigenetic modifications, thereby playing crucial biological roles. During transcription, tsRNAs identify target mRNA and compete to bind with it. They replace the untranslated regions in mRNA, thereby reducing the stability of the transcript and consequently inhibits mRNA expression [71]. In this article, to explore and estimate whether tsRNA can serve as a diagnostic marker for NPC, we used small RNA microarray profiling and array hybridization to screen for specific tsRNA in NPC serum. As a result, we identified 9 differently upregulated tsRNAs, namely 5′tiRNA-32-ValAAC-2, tRF5-50-GlyGCC-2, i-tRF-4:24-His-GTG-1, i-tRF-2:25-His-GTG-1, 5′tiRNA-35-GlnTTG-6, tRF5-31-HisGTG-1, tRF5-23-HisGTG-1, 5′tiRNA-34-GlnTTG-6, and mt-tRF5-26-LeuTAA, and verified that they have certain value for the primary diagnosis of NPC. Among them, 5′tiRNA-32-ValAAC-2 has the greatest clinical significance, so this tsRNA was further investigated. The results indicated that 5′tiRNA-32-ValAAC-2 may be a novel potential biomarker.

To further define the clinical significance of these 9 specific tsRNAs, RT-qPCR was initially employed to validate their expressions in the sera of NPC patients compared with normal individuals. Except that 5′tiRNA-35-GlnTTG-6 showed non-significant upregulation, the remaining 8 candidate tsRNAs were all significantly upregulated in newly diagnosed NPC patients. In ROC analysis of validated tsRNAs, based on the criterion of AUC $\geqslant$ 0.950, we considered tRF5-23-HisGTG-1, 5′tiRNA-32-ValAAC-2, tRF5-31-HisGTG-1 and i-tRF-2:25-His-GTG-1 as potential diagnostic biomarkers for newly diagnosed NPC. 5′tiRNA-32-ValAAC-2 is a member of cytoplasmic tRNAs and is located chr5q35.3. In line with previous findings, patients with liver cancer exhibited significantly higher levels of tRNA-ValAAC-5 in plasma exosome [72], which underscores the potential of 5′tRNA-ValAAC as a promising biomarker for NPC diagnosis. Meanwhile, lactic acid dramatically enhances the ratio of 5′tRNAHis and 5′tRNAVal [73], impairing the EBV-infected B cell lymphoma cells cycle and proliferation, which means that the 5′tRNAHis can also serve as a novel molecular target for NPC diagnosis and treatment. tRF5-23-HisGTG-1 and tRF5-31-HisGTG-1 are members of 5′tRNAHis family, while i-tRF-2:25-His-GTG-1 belongs to the His tRNAs family. All of the tRF5-23-HisGTG-1, tRF5-31-HisGTG-1 and i-tRF-2:25-His-GTG-1 are part of HisGTG tRF family. As reported, the HisGTG tRF is enriched in the non-nuclear fraction and highly concentrated in mitochondria, where it regulates mitochondrial function [74]. tiRNA-HisGTG, exerting a regulatory function with mitochondrial oxidative stress [75], strongly suggests that tiRNAs, known as stress-induced tRNAs, are derived from mature tRNAs cleaved by ANG at the anticodon ring [13]. The level of 5′tiRNA-His-GTG is upregulated in NPC sera, which is consistent with the situation in colorectal cancer tissues [76]. Targeting 5′tiRNA-His-GTG can modulate the response process of the tumor hypoxic microenvironment, thereby inducing cell apoptosis [76]. Apart from this, 5′tiRNA-His-GTG can also perform the above functions through osthole [77] and quercetin [78]. Therefore, 5′tiRNA-His-GTG may serve as a potential therapeutic target for NPC patients. Moreover, 5′tiRNA and tRF5 may exert an important role in the development and progression of NPC.

In addition, both 5′tiRNA and tRF5 belong to 5′-tRFs. Mechanistically, their biological functions are mainly associated with gene silencing, translation regulation, and epigenetic modification regulation [79]. It has been verified that 5′tiRNA-His-GTG acts as a crucial regulator of retinal neurovascular dysfunction, primarily by modulating arachidonic acid (AA) metabolism through the cytochrome P450 enzymes (CYPs) pathway [80]. 5′tiRNA-Gly-GCC modulated the *JAK1*/*STAT6* signaling pathway by targeting *SPIB*. Poly (β-amino esters) were synthesized to assist the delivery of 5-FU and 5′tiRNA-Gly-GCC inhibitor, which effectively inhibited tumor growth and enhanced the sensitivity of CRC to 5-FU [81]. Additionally, 5′tiRNA-Gly dysregulated the expression of downstream genes related to inflammatory response, the activation of satellite cells, and the differentiation of myoblasts through the *TGF-β* signaling pathway by targeting *Tgfbr1* [82]. One finding revealed that

5′-tiRNA-Cys-GCA is a potential regulator of the Alzheimer's disease (AD) pathological process via the *STAT4* signaling pathway [83]. Another finding indicated that 5′-tiRNA-Gln interacts with *EIF4A1* to reduce related mRNA binding through the intramolecular G-quadruplex structure, and this process partially inhibits translation and the progression of hepatocellular carcinoma [84]. Our research discovered that overexpression of 5′tiRNA-32-ValAAC-2 facilitates the proliferation, migration and invasion ability of NPC cells. Although 5′tiRNA-32-ValAAC-2 has not been previously reported, our findings and the latest studies on the 5′tiRNA mechanism imply that 5′tiRNA-32-ValAAC-2 may be a novel pathogenic factor for NPC. It is possible that 5′tiRNA-32-ValAAC-2 participates in the development of NPC and plays a crucial role in tumorigenesis.

Using TargetScan and miRanda, we identified the top 5 most relevant genes of 5′tiRNA-32-ValAAC-2, namely *UGT2B7*, *SYNPO2*, *ZNF44*, *PDHB*, *UFM1*. Estrogen homeostasis is regulated by *UGT2B7*, and it promotes the migration and invasion of breast cancer cells, causing the development of breast cancer metastasis [52]. *SYNPO2* plays a pivotal role in regulating tumor growth, development and progression in bladder urothelial carcinoma [54] and fibrosarcoma [55]. *ZNF44* can promote neuroblastoma growth and invasion as potential driver mutations [56]. The overexpression of *PDHB* can inhibit the proliferation, migration, and invasion of renal clear cell carcinoma [57] and cervical cancer [58]. An elevated level of *UFM1* is associated with the proliferation, migration and invasion of cancer cells [59,60].

In summary, we used small RNA microarray profiling and array hybridization to detect the expression spectrums of tsRNAs in the sera of newly diagnosed NPC patients. It was verified that 5′tiRNA-32-ValAAC-2, tRF5-23-HisGTG-1, tRF5-31-HisGTG-1, and i-tRF-2:25-His-GTG-1 could serve as potential diagnostic biomarkers for NPC. As a crucial tsRNA for the diagnosis of NPC, 5′tiRNA-32-ValAAC-2 holds significant research value and scientific innovation. The most relevant genes of 5′tiRNA-32-ValAAC-2 are *UGT2B7*, *SYNPO2*, *ZNF44*, *PDHB*, *UFM1*. Through the CCK-8 assay and clone formation assay, we discovered that the overexpression of 5′tiRNA-32-ValAAC-2 promotes the proliferation of NPC cells. Furthermore, via wound healing assay and Transwell assay, it was found that the overexpression of 5′tiRNA-32-ValAAC-2 can enhance the migration and invasion capabilities of NPC cells.

Conclusions

In this study, the tsRNA spectrums of serum from NPC patients were analyzed. It was verified that 5′tiRNA-32-ValAAC-2 is a pathogenic molecule and a potential diagnostic biomarker for NPC. The genes most closely associated with 5′tiRNA-32-ValAAC-2 are *UGT2B7*, *SYNPO2*, *ZNF44*, *PDHB*, *UFM1*. Overexpression of 5′tiRNA-32-ValAAC-2 promotes the proliferation, migration, and invasion of NPC cells. On the contrary, inhibition of 5′tiRNA-32-ValAAC-2 suppresses the proliferation, migration, and invasion of NPC cells. 5′tiRNA-32-ValAAC-2 may serve as a novel diagnostic biomarker in primary NPC and a therapeutic target molecule.

Acknowledgements

We thank Professor Qianjin Liao from the Medical Research Center of Hunan Cancer Hospital and Xiangya School of Medicine of Central South University for his contributions. This work was supported in part by the Major Science and Technological Innovation Project of Hunan Province (No. 2021SK1020-4), and the Pandeng Project of Hunan Cancer Hospital (No. YF2020001).

Compliance with ethics guidelines

Conflicts of interest Qi Tang, Yao Wu, Lin Chen, Qunying Jia, Yingchun He, and Faqing Tang declare no competing financial interests.

The study was approved by the Ethics Committee of the Hunan Cancer Hospital and Institute (No.2024 [30], Supplementary file 1) and the study was performed in accordance with the ethical standards as laid down in the 1964 Declaration of Helsinki and its later amendments or comparable ethical standards. Informed consent was obtained from all patients for being included in the study.

Data availability and compliance statement

The authors declare that the acquisition and subsequent use of all data presented in this manuscript fully comply with all relevant local, national, and international laws, regulations, ethical guidelines, and the terms of use associated with the original data sources.

The authors bear full legal responsibility for ensuring the legality of data acquisition and all subsequent uses of the data.

The datasets generated and analyzed during the current study are available from the corresponding author on reasonable request.

Electronic supplementary material Supplementary material is available in the online version of this article at https://doi.org/10.1007/s11684-025-1175-x and is accessible for authorized users.

References

1. Filho AM, Laversanne M, Ferlay J, Colombet M, Piñeros M, Znaor

A, Parkin DM, Soerjomataram I, Bray F. The GLOBOCAN 2022 cancer estimates: data sources, methods, and a snapshot of the cancer burden worldwide. Int J Cancer 2025; 156(7): 1336–1346
2. Han B, Zheng R, Zeng H, Wang S, Sun K, Chen R, Li L, Wei W, He J. Cancer incidence and mortality in China, 2022. J Natl Cancer Cent 2024; 4(1): 47–53
3. Chen YP, Chan ATC, Le QT, Blanchard P, Sun Y, Ma J. Nasopharyngeal carcinoma. Lancet 2019; 394(10192): 64–80
4. Zhang X, Chen Y, Liang J, Yang Y, Chen H, Chen Z, Li M, Chen S, Chen T, He H, Liu Y, Liu Z, Han L, Wu D, Zou Z, Qu Y, Li M, Stoneking M, Fu Q, Xu S, Zeng YX, Ma L, Liu J, Xu M, Zhai W. Out-of-Africa migration and clonal expansion of a recombinant Epstein-Barr virus drives frequent nasopharyngeal carcinoma in southern China. Natl Sci Rev 2024; 12(4): nwae438
5. Li H, Wang X, Sun A, Liu W, Lv R, Zhang M, Xing Z, Ma S, Liu Y, Zhang K. tRF-1: 28-Val-CAC-2 promotes the development of nasopharyngeal cancer by targeting EPHB2. Front Oncol 2025; 15: 1564601
6. Lu Z, Su K, Wang X, Zhang M, Ma S, Li H, Qiu Y. Expression profiles of tRNA-derived small RNAs and their potential roles in primary nasopharyngeal carcinoma. Front Mol Biosci 2021; 8: 780621
7. Chen Q, Li D, Jiang L, Wu Y, Yuan H, Shi G, Liu F, Wu P, Jiang K. Biological functions and clinical significance of tRNA-derived small fragment (tsRNA) in tumors: current state and future perspectives. Cancer Lett 2024; 587: 216701
8. Li Z, Zhang B, Pan Y, Weng Q, Hu K. Emerging roles of tsRNAs in programmed cell death and disease therapeutics: challenges, opportunities, and future directions. Noncoding RNA Res 2025; 15: 65–73
9. Phizicky EM, Hopper AK. tRNA biology charges to the front. Genes Dev 2010; 24(17): 1832–1860
10. Frank DN, Pace NR. Ribonuclease P: unity and diversity in a tRNA processing ribozyme. Annu Rev Biochem 1998; 67(1): 153–180
11. Dubrovsky EB, Dubrovskaya VA, Levinger L, Schiffer S, Marchfelder A. Drosophila RNase Z processes mitochondrial and nuclear pre-tRNA 3′ ends *in vivo*. Nucleic Acids Res 2004; 32(1): 255–262
12. Maraia RJ, Lamichhane TN. 3′ processing of eukaryotic precursor tRNAs. Wiley Interdiscip Rev RNA 2011; 2(3): 362–375
13. Xie Y, Yao L, Yu X, Ruan Y, Li Z, Guo J. Action mechanisms and research methods of tRNA-derived small RNAs. Signal Transduct Target Ther 2020; 5(1): 109
14. Yamasaki S, Ivanov P, Hu GF, Anderson P. Angiogenin cleaves tRNA and promotes stress-induced translational repression. J Cell Biol 2009; 185(1): 35–42
15. Fu M, Gu J, Wang M, Zhang J, Chen Y, Jiang P, Zhu T, Zhang X. Emerging roles of tRNA-derived fragments in cancer. Mol Cancer 2023; 22(1): 30
16. Tao EW, Cheng WY, Li WL, Yu J, Gao QY. tiRNAs: A novel class of small noncoding RNAs that helps cells respond to stressors and plays roles in cancer progression. J Cell Physiol 2020; 235(2): 683–690
17. Shen Y, Yu X, Zhu L, Li T, Yan Z, Guo J. Transfer RNA-derived fragments and tRNA halves: biogenesis, biological functions and their roles in diseases. J Mol Med (Berl) 2018; 96(11): 1167–1176
18. Zhu L, Ge J, Li T, Shen Y, Guo J. tRNA-derived fragments and tRNA halves: the new players in cancers. Cancer Lett 2019; 452: 31–37
19. Liao JY, Ma LM, Guo YH, Zhang YC, Zhou H, Shao P, Chen YQ, Qu LH. Deep sequencing of human nuclear and cytoplasmic small RNAs reveals an unexpectedly complex subcellular distribution of miRNAs and tRNA 3′ trailers. PLoS One 2010; 5(5): e10563
20. Kumar P, Kuscu C, Dutta A. Biogenesis and function of transfer RNA-related fragments (tRFs). Trends Biochem Sci 2016; 41(8): 679–689
21. Yu X, Xie Y, Zhang S, Song X, Xiao B, Yan Z. tRNA-derived fragments: mechanisms underlying their regulation of gene expression and potential applications as therapeutic targets in cancers and virus infections. Theranostics 2021; 11(1): 461–469
22. Kumar P, Anaya J, Mudunuri SB, Dutta A. Meta-analysis of tRNA derived RNA fragments reveals that they are evolutionarily conserved and associate with AGO proteins to recognize specific RNA targets. BMC Biol 2014; 12(1): 78
23. Wang Q, Pan Z, Liang S, Shi Y, Dong G, Xu L, Mao Q, Jiang F. Transfer RNA-derived small RNAs (tsRNAs): a rising star in liquid biopsy. Genes Dis 2025; 12(5): 101608
24. Uchida Y, Chiba T, Kurimoto R, Asahara H. Post-transcriptional regulation of inflammation by RNA-binding proteins via cis-elements of mRNAs. J Biochem 2019; 166(5): 375–382
25. Boskovic A, Bing XY, Kaymak E, Rando OJ. Control of noncoding RNA production and histone levels by a 5′ tRNA fragment. Genes Dev 2020; 34(1-2): 118–131
26. Kim HK. Transfer RNA-derived small non-coding RNA: dual regulator of protein synthesis. Mol Cells 2019; 42(10): 687–692
27. Chen Q, Zhang X, Shi J, Yan M, Zhou T. Origins and evolving functionalities of tRNA-derived small RNAs. Trends Biochem Sci 2021; 46(10): 790–804
28. Li D, Gao X, Ma X, Wang M, Cheng C, Xue T, Gao F, Shen Y, Zhang J, Liu Q. Aging-induced $tRNA^{Glu}$-derived fragment impairs glutamate biosynthesis by targeting mitochondrial translation-dependent cristae organization. Cell Metab 2024; 36(5): 1059–1075.e9
29. Fan Y, Pavani KC, Smits K, Van Soom A, Peelman L. tRNAGlu-derived fragments from embryonic extracellular vesicles modulate bovine embryo hatching. J Anim Sci Biotechnol 2024; 15(1): 23
30. Xiong Q, Zhang Y, Xu Y, Yang Y, Zhang Z, Zhou Y, Zhang S, Zhou L, Wan X, Yang X, Zeng Z, Liu J, Zheng Y, Han J, Zhu Q. tiRNA-Val-CAC-2 interacts with FUBP1 to promote pancreatic cancer metastasis by activating c-MYC transcription. Oncogene 2024; 43(17): 1274–1287
31. Tan L, Wu X, Tang Z, Chen H, Cao W, Wen C, Zou G, Zou H. The tsRNAs (tRFdb-3013a/b) serve as novel biomarkers for colon adenocarcinomas. Aging (Albany NY) 2024; 16(5): 4299–4326
32. Xu T, Yuan J, Song F, Zhang N, Gao C, Chen Z. Exploring the functional role of tRF-39–8HM2OSRNLNKSEKH9 in hepatocellular carcinoma. Heliyon 2024; 10(5): e27153
33. Ding M, Zhou W, Chen W, Mo W, Guo X, Li Y, Ji C, Liu G, Diao W, Guo H. Plasma tsRNAs as novel diagnostic biomarkers for renal cell carcinoma. Clin Transl Med 2024; 14(2): e1575
34. Xu J, Wang Y, Li X, Zheng M, Li Y, Zhang W. Clinical value assessment for serum hsa_tsr013526 in the diagnosis of gastric carcinoma. Environ Toxicol 2024; 39(5): 2753–2767
35. Liu L, Xu Z, Dai X, Zhou X, Chen L, Luan C, Huang D, Chen H, Zhang J, Hu Y, Chen K. Mechanistic insights into 5′-tiRNA-His-

GTG mediated activation of the JNK pathway in skin photoaging. Aging Cell 2025; 24(7): e70049
36. Jirström E, Matveeva A, Baindoor S, Donovan P, Ma Q, Morrissey EP, Arijs I, Boeckx B, Lambrechts D, Garcia-Munoz A, Dillon ET, Wynne K, Ying Z, Matallanas D, Hogg MC, Prehn JHM. Effects of ALS-associated 5′tiRNAGly-GCC on the transcriptomic and proteomic profile of primary neurons in vitro. Exp Neurol 2025; 385: 115128
37. Xu N, Huang J, Wang Y, Liu Y, Jiang Y, Zhou W, Sheng J, Zhang L. 5′-tiRNA-Lys maintains intestinal epithelial homeostasis by EWSR1-dependent suppression of miR-125a and autophagy activation. Acta Biochim Biophys Sin (Shanghai) 2025; [Epub ahead of print] doi: 10.3724/abbs.2025074
38. Tzur Y, Winek K, Madrer N, Dubnov S, Bennett ER, Greenberg DS, Hanin G, Gammal A, Tam J, Arkin IT, Paldor I, Soreq H. Lysine tRNA fragments and miR-194-5p co-regulate hepatic steatosis via β-Klotho and perilipin 2. Mol Metab 2024; 79: 101856
39. Xu Z, Liu L, Dai X, Zhou X, Chen L, Chen H, Luan C, Huang D, Zhang J, Hu Y, Chen K, Gu H. 5'tiRNA-Glu-TTC targets TRPV3 and activates the PI3K/AKT signaling pathway to modulate skin photoaging. Noncoding RNA Res 2025; 15: 29–43
40. Liu R, Zhang L, Hu P, Liu A, Zhang Y, Liu Q, Guo J, Han D, Yue H, Zhang B. 5′tiRNA-35-GlyTCC-3 and 5′tiRNA-33-CysGCA-11 target BMP6, CUL1 and SPR of non-syndromic cleft palate. BMC Oral Health 2025; 25(1): 307
41. Wang J, Liu X, Cui W, Gao Y, Zhang C, Duan C. Plasma tRNA-derived small RNAs signature as a predictive and prognostic biomarker in lung adenocarcinoma. Cancer Cell Int 2022; 22(1): 59
42. Xu C, Fu Y. Expression profiles of tRNA-derived fragments and their potential roles in multiple myeloma. OncoTargets Ther 2021; 14: 2805–2814
43. Veneziano D, Tomasello L, Balatti V, Palamarchuk A, Rassenti LZ, Kipps TJ, Pekarsky Y, Croce CM. Dysregulation of different classes of tRNA fragments in chronic lymphocytic leukemia. Proc Natl Acad Sci USA 2019; 116(48): 24252–24258
44. Mendonca T, Urban R, Lucken K, Coney G, Kad NM, Tassieri M, Wright AJ, Booth DG. The mitotic chromosome periphery modulates chromosome mechanics. Nat Commun 2025; 16(1): 6399
45. Andrés-Sánchez N, Fisher D, Krasinska L. Physiological functions and roles in cancer of the proliferation marker Ki-67. J Cell Sci 2022; 135(11): jcs258932
46. Mrouj K, Andrés-Sánchez N, Dubra G, Singh P, Sobecki M, Chahar D, Al Ghoul E, Aznar AB, Prieto S, Pirot N, Bernex F, Bordignon B, Hassen-Khodja C, Villalba M, Krasinska L, Fisher D. Ki-67 regulates global gene expression and promotes sequential stages of carcinogenesis. Proc Natl Acad Sci USA 2021; 118(10): e2026507118
47. Yang C, Zhang J, Ding M, Xu K, Li L, Mao L, Zheng J. Ki67 targeted strategies for cancer therapy. Clin Transl Oncol 2018; 20(5): 570–575
48. Gürsoy G. CRP/albumin ratio and WBC values correlate with Ki-67 and survival in glioblastoma multiforme. Front Oncol 2025; 15: 1612212
49. Tian K, Tong P, Wu K, Azhar A, Fang Y, Xu N, Wang R. Development of a model to predict Ki-67 expression status in non-Hodgkin's lymphoma based on PET radiomics. Front Oncol 2025; 15: 1567152
50. Chen S, Dai J, Zhao J, Han S, Zhang X, Chang J, Jiang D, Zhang H, Wang P, Hu S. Synthetic MRI combined with clinicopathological characteristics for pretreatment prediction of chemoradiotherapy response in advanced nasopharyngeal carcinoma. Korean J Radiol 2025; 26(2): 135–145
51. Guo C, Luo J, Liang M, Xiao J. Correlation of 18 F-FDG PET/CT metabolic parameters with Ki-67 expression and tumor staging in nasopharyngeal carcinoma. Nucl Med Commun 2025; 46(5): 437–443
52. Xu J, Zhou Y, He S, Wang Y, Ma J, Li C, Liu Z, Zhou X. Activation of the YY1–UGT2B7 axis promotes mammary estrogen homeostasis dysregulation and exacerbates breast tumor metastasis. Drug Metab Dispos 2024; 52(5): 408–421
53. Ondo K, Isono M, Nakano M, Hashiba S, Fukami T, Nakajima M. The N^6-methyladenosine modification posttranscriptionally regulates hepatic UGT2B7 expression. Biochem Pharmacol 2021; 189: 114402
54. Ye G, Tu L, Li Z, Li X, Zheng X, Song Y. $SYNPO_2$ promotes the development of BLCA by upregulating the infiltration of resting mast cells and increasing the resistance to immunotherapy. Oncol Rep 2024; 51(1): 14
55. Cheng X, Xu J, Gu H, Chen G, Wu L. ALDH1+ tumor stem cells promote the progression of malignant fibrous tissue sarcoma by inhibiting SYNPO2 through hsa-mir-206. Exp Cell Res 2024; 441(1): 114167
56. Esposito MR, Binatti A, Pantile M, Coppe A, Mazzocco K, Longo L, Capasso M, Lasorsa VA, Luksch R, Bortoluzzi S, Tonini GP. Somatic mutations in specific and connected subpathways are associated with short neuroblastoma patients' survival and indicate proteins targetable at onset of disease. Int J Cancer 2018; 143(10): 2525–2536
57. Wu J, Wang S, Liu Y, Zhang T, Wang X, Miao C. Integrated single-cell and bulk characterization of cuproptosis key regulator PDHB and association with tumor microenvironment infiltration in clear cell renal cell carcinoma. Front Immunol 2023; 14: 1132661
58. Chi C, Hou W, Zhang Y, Chen J, Shen Z, Chen Y, Li M. PDHB-AS suppresses cervical cancer progression and cisplatin resistance via inhibition on Wnt/β-catenin pathway. Cell Death Dis 2023; 14(2): 90
59. Ke D, Guo HH, Jiang N, Shi RS, Fan TY. Inhibition of UFM1 expression suppresses cancer progression and is linked to the dismal prognosis and immune infiltration in oral squamous cell carcinoma. Aging (Albany NY) 2023; 15(22): 13059–13076
60. Mao M, Chen Y, Yang J, Cheng Y, Xu L, Ji F, Zhou J, Zhang X, Li Z, Chen C, Ju S, Zhang J, Wang L. Modification of PLAC8 by UFM1 affects tumorous proliferation and immune response by impacting PD-L1 levels in triple-negative breast cancer. J Immunother Cancer 2022; 10(12): e005668
61. Xie L, Zhang K, You B, Yin H, Zhang P, Shan Y, Gu Z, Zhang Q. Hypoxic nasopharyngeal carcinoma-derived exosomal miR-455 increases vascular permeability by targeting ZO-1 to promote metastasis. Mol Carcinog 2023; 62(6): 803–819
62. Hu W, Wang Y, Zhang Q, Luo Q, Huang N, Chen R, Tang X, Li X, Luo H. MicroRNA-199a-3p suppresses the invasion and metastasis of nasopharyngeal carcinoma through SCD1/PTEN/AKT signaling pathway. Cell Signal 2023; 110: 110833

63. Zhang C, Chen W, Pan S, Zhang S, Xie H, Zhang Z, Lei W, Bao L, You Y. SEVs-mediated miR-6750 transfer inhibits pre-metastatic niche formation in nasopharyngeal carcinoma by targeting M6PR. Cell Death Discov 2023; 9(1): 2
64. Tian Y, Ai M, Liu C, Wu Y, Khan M, Wang B, Long H, Huang C, Lin J, Xu A, Li R, Cen B, Qiu W, Xie G, Yuan Y. Upregulated long non-coding RNA lnc-MRPL39-2: 1 induces the growth and invasion of nasopharyngeal carcinoma by binding to HuR and stabilizing β-catenin mRNA. Int J Biol Sci 2023; 19(8): 2349–2365
65. Liu H, Chen Q, Zheng W, Zhou Y, Bai Y, Pan Y, Zhang J, Shao C. LncRNA CASC19 enhances the radioresistance of nasopharyngeal carcinoma by regulating the miR-340-3p/FKBP5 axis. Int J Mol Sci 2023; 24(3): 3047
66. Peng Y, Zhang Y, Liu Y, Dong Z, Wang T, Peng F, Di W, Zong D, Du M, Zhou H, He X. LINC01376 promotes nasopharyngeal carcinoma tumorigenesis by competitively binding to the SP1/miR-4757/IGF1 axis. IUBMB Life 2023; 75(9): 702–716
67. Mo Y, Wang Y, Zhang S, Xiong F, Yan Q, Jiang X, Deng X, Wang Y, Fan C, Tang L, Zhang S, Gong Z, Wang F, Liao Q, Guo C, Li Y, Li X, Li G, Zeng Z, Xiong W. Circular RNA circRNF13 inhibits proliferation and metastasis of nasopharyngeal carcinoma via SUMO2. Mol Cancer 2021; 20(1): 112
68. Li Q, Zhao YH, Xu C, Liang YL, Zhao Y, He QM, Li JY, Chen KL, Qiao H, Liu N, Ma J, Chen L, Li YQ. Chemotherapy-induced senescence reprogramming promotes nasopharyngeal carcinoma metastasis by circRNA-mediated PKR activation. Adv Sci (Weinh) 2023; 10(8): 2205668
69. Hong X, Li Q, Li J, Chen K, He Q, Zhao Y, Liang Y, Zhao Y, Qiao H, Liu N, Ma J, Li Y. CircIPO7 promotes nasopharyngeal carcinoma metastasis and cisplatin chemoresistance by facilitating YBX1 nuclear localization. Clin Cancer Res 2022; 28(20): 4521–4535
70. Mao M, Chen W, Huang X, Ye D. Role of tRNA-derived small RNAsn (tsRNAs) in the diagnosis and treatment of malignant tumours. Cell Commun Signal 2023; 21(1): 178
71. Chen Y, Tang Y, Hou S, Luo J, Chen J, Qiu H, Chen W, Li K, He J, Li J. Differential expression spectrum and targeted gene prediction of tRNA-derived small RNAs in idiopathic pulmonary arterial hypertension. Front Mol Biosci 2023; 10: 1204740
72. Zhu L, Li J, Gong Y, Wu Q, Tan S, Sun D, Xu X, Zuo Y, Zhao Y, Wei YQ, Wei XW, Peng Y. Exosomal tRNA-derived small RNA as a promising biomarker for cancer diagnosis. Mol Cancer 2019; 18(1): 74
73. Mo X, Du S, Chen X, Wang Y, Liu X, Zhang C, Zhu C, Ding L, Li Y, Tong Y, Ju Q, Qu D, Tan F, Wei F, Cai Q. Lactate induces production of the tRNAHis half to promote B-lymphoblastic cell proliferation. Mol Ther 2020; 28(11): 2442–2457
74. Bayazit MB, Jacovetti C, Cosentino C, Sobel J, Wu K, Brozzi F, Rodriguez-Trejo A, Stoll L, Guay C, Regazzi R. Small RNAs derived from tRNA fragmentation regulate the functional maturation of neonatal β cells. Cell Rep 2022; 40(2): 111069
75. Ham J, Park W, Song J, Kim HS, Song G, Lim W, Park SJ, Park S. Fraxetin reduces endometriotic lesions through activation of ER stress, induction of mitochondria-mediated apoptosis, and generation of ROS. Phytomedicine 2024; 123: 155187
76. Tao EW, Wang HL, Cheng WY, Liu QQ, Chen YX, Gao QY. A specific tRNA half, 5′tiRNA-His-GTG, responds to hypoxia via the HIF1α/ANG axis and promotes colorectal cancer progression by regulating LATS2. J Exp Clin Cancer Res 2021; 40(1): 67
77. Song J, Ham J, Park W, Song G, Lim W. Osthole impairs mitochondrial metabolism and the autophagic flux in colorectal cancer. Phytomedicine 2024; 125: 155383
78. Yang C, Song J, Park S, Ham J, Park W, Park H, An G, Hong T, Kim HS, Song G, Lim W. Targeting thymidylate synthase and tRNA-derived non-coding RNAs improves therapeutic sensitivity in colorectal cancer. Antioxidants 2022; 11(11): 2158
79. Hu Y, Cai A, Xu J, Feng W, Wu A, Liu R, Cai W, Chen L, Wang F. An emerging role of the 5′ termini of mature tRNAs in human diseases: current situation and prospects. Biochim Biophys Acta Mol Basis Dis 2022; 1868(2): 166314
80. Yao J, Yao W, Zhu JY, Liu Y, Liu JH, Ji YK, Ni XS, Mu W, Yan B. Targeting tRNA-derived non-coding RNA alleviates diabetes-induced visual impairment through protecting retinal neurovascular unit. Adv Sci (Weinh) 2025; 12(1): e2411042
81. Xu R, Du A, Deng X, Du W, Zhang K, Li J, Lu Y, Wei X, Yang Q, Tang H. tsRNA-GlyGCC promotes colorectal cancer progression and 5-FU resistance by regulating SPIB. J Exp Clin Cancer Res 2024; 43(1): 230
82. Shen L, Liao T, Chen Q, Lei Y, Wang L, Gu H, Qiu Y, Zheng T, Yang Y, Wei C, Chen L, Zhao Y, Niu L, Zhang S, Zhu Y, Li M, Wang J, Li X, Gan M, Zhu L. tRNA-derived small RNA, 5′tiRNA-Gly-CCC, promotes skeletal muscle regeneration through the inflammatory response. J Cachexia Sarcopenia Muscle 2023; 14(2): 1033–1045
83. Zong T, Yang Y, Lin X, Jiang S, Zhao H, Liu M, Meng Y, Li Y, Zhao L, Tang G, Gong K, Wang Z, Yu T. 5′-tiRNA-Cys-GCA regulates VSMC proliferation and phenotypic transition by targeting STAT4 in aortic dissection. Mol Ther Nucleic Acids 2021; 26: 295–306
84. Wu C, Liu D, Zhang L, Wang J, Ding Y, Sun Z, Wang W. 5′-tiRNA-Gln inhibits hepatocellular carcinoma progression by repressing translation through the interaction with eukaryotic initiation factor 4A-I. Front Med 2023; 17(3): 476–492